International Journal of Biological Macromolecules 249 (2023) 125918

Contents lists available at ScienceDirect

International Journal of Biological Macromolecules

journal homepage: www.elsevier.com/locate/ijbiomac

Fabrication of a protein-dextran conjugates formed oral nanoemulsion and its application to deliver the essential oil from *Alpinia zerumbet* Fructus

Jinzhuan Xu [a,b,1], Zhaohui Jiang [c,1], Jianqing Peng [a,b,1], Runbin Sun [d], Lili Zhang [a], Yan Chen [a,b], Di Pan [a,b], Jing Huang [a], Zipeng Gong [a,*], Yi Chen [a,b,**], Xiangchun Shen [a,b,**]

[a] The State Key Laboratory of Functions and Applications of Medicinal Plants, School of Pharmaceutical Sciences, Guizhou Medical University, Guiyang 550025, China
[b] The High Efficacy Application of Natural Medicinal Resources Engineering Center of Guizhou Province, School of Pharmaceutical Sciences, Guizhou Medical University, Guiyang 550025, China
[c] The First People's Hospital of Guiyang, Guiyang 550002, China
[d] Phase I Clinical Trials Unit, Nanjing Drum Tower Hospital, Affiliated Hospital of Medical School, Nanjing University, Nanjing 210008, China

ARTICLE INFO

Keywords:
Proteoglycan based nanoemulsion
Vascular endothelial injury
Essential oil from *Alpinia zerumbet* Fructus (EOFAZ)

ABSTRACT

The injury of vascular endothelial cells caused by high glucose (HG) is one of the driving factors of vascular complications of diabetes. Oral administration is the most common route of administration for the treatment of diabetes and its vascular complications. Essential oil extracts from Chinese medicine possess potential therapeutic effects on vascular endothelial injury. However, low solubility and volatility of essential oils generally result in poor oral absorption. Development of nanocarriers for essential oils is a promising strategy to overcome the physiological barriers of oral absorption. In this study, a nanoemulsion composed of bovine serum albumin (BSA)-dextran sulfate (DS) conjugate and sodium deoxycholate (SD) was constructed. The nanoemulsions were verified with promoted oral absorption and prolonged circulation time. After the primary evaluation of the nanoemulsion, essential oil from *Alpinia zerumbet* Fructus (EOFAZ)-loaded nanoemulsion (denoted as EOFAZ@BD_5/S) was prepared and characterized. Compared to the free EOFAZ, EOFAZ@BD_5/S increased the protective effects on HG-induced HUVEC injury *in vitro* and ameliorative effects on the vascular endothelium disorder and tunica media fibroelastosis in a T_2DM mouse model. Collectively, this study provides a nanoemulsion for the oral delivery of essential oils, which holds strong promise in the treatment of diabetes-induced vascular endothelial injury.

1. Introduction

The multiple complications of diabetes are the leading cause of death [1,2]. Complications of diabetes are usually divided into macrovascular complications (such as cardiovascular disease) and microvascular complications (such as affecting the kidneys, retina, nervous system, *etc.*) [3,4]. Hyperglycemia causes oxidative stress and inflammation, which in turn leads to damage and dysfunction of vascular endothelial cells [3,5]. This is thought to be the initiating factor in vascular complications. Traditional Chinese medicine has a long history in the prevention and treatment of cardiovascular and cerebrovascular diseases, and has the advantages of safety, low toxicity and high safety [6,7]. As important active compounds of Chinese medicine, essential oils with anti-inflammatory, antioxidant and oxygen free radical scavenging activities [8,9] hold strong promise in preventing hyperglycemia-induced vascular endothelial injury.

Since diabetes requires lifelong medication, it is suggested that oral administration with good compliance is the most common route in the treatment of diabetes. Due to the poor water solubility and instability of drugs and the complex gastrointestinal environment, essential oils

* Correspondence to: Z. Gong, The State Key Laboratory of Functions and Applications of Medicinal Plants, School of Pharmaceutical Sciences, Guizhou Medical University, Guiyang 550025, China.
** Corresponding authors at: The State Key Laboratory of Functions and Applications of Medicinal Plants, School of Pharmaceutical Sciences, Guizhou Medical University, Guiyang 550025, China. The High Efficacy Application of Natural Medicinal Resources Engineering Center of Guizhou Province, School of Pharmaceutical Sciences, Guizhou Medical University, Guiyang 550025, China.
E-mail addresses: gzp4012607@126.com (Z. Gong), chenyi_19890319@126.com (Y. Chen), shenxiangchun@126.com (X. Shen).
[1] Jinzhuan Xu, Zhaohui Jiang and Jianqing Peng contributed equally to this work.

https://doi.org/10.1016/j.ijbiomac.2023.125918
Received 28 January 2023; Received in revised form 4 July 2023; Accepted 18 July 2023
Available online 24 July 2023

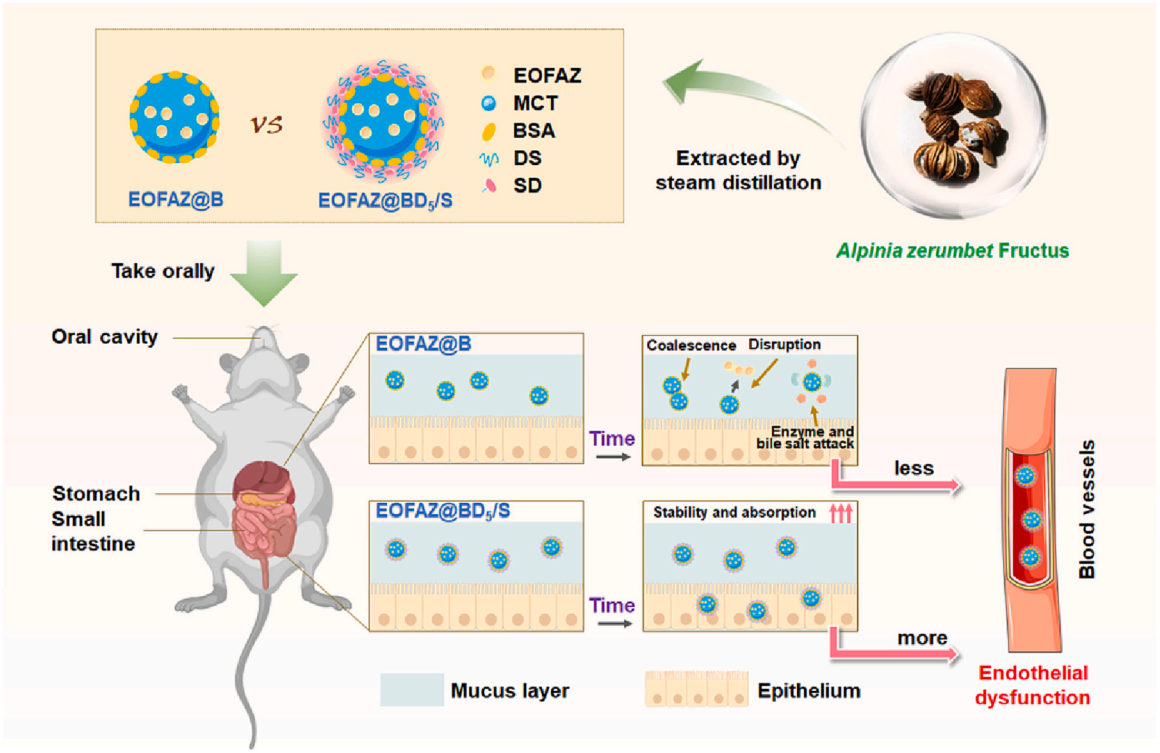

Scheme 1. Schematic illustration of nanoemulsions promoting oral absorption of EOFAZ. EOFAZ@BD_5/S increases protection against vascular injury by promoting oral absorption of EOFAZ, prolonging circulation time, and increasing focal site aggregation.

exhibit poor oral absorption and low bioavailability [10,11]. Various drug delivery systems, including lipid nanoparticles [12], nanoemulsions [13,14], chitosan-based hydrogels [15–17], and cellulose nanocrystals [18], have been reported in recent decades to improve the solubility and stability of essential oils. Among them, nanoemulsion with good biocompatibility and stability is an ideal carrier for essential oils, which can effectively reduce the volatilization and degradation of essential oils due to the mixture with the oil phase.

Proteins are good emulsifiers that can diffuse at the oil-water interface to form a viscoelastic interface film [19]. Bovine serum albumin (BSA) has been widely used to prepare nanoemulsions [20]. However, the interfacial film formed by BSA alone is not stable enough to resist environmental factors such as pH, ionic strength, and temperature [21]. Since polysaccharides can form extended spatial network structures and increase steric hindrance between emulsion droplets, protein-polysaccharide complexes can be used as emulsifiers to enhance the stability of nanoemulsions [22,23]. It is reported that dextran sulfate (DS) is a ligand of scavenger receptor-collectin placenta 1 (CL-P1), which is overexpressed on the damaged vascular endothelial cells. Therefore, DS was conjugated with BSA to obtain a protein-dextran emulsifier BSA-DS (BD) [24–26]. This emulsifier possessed enhanced emulsifying capability compared with BSA and damaged vascular endothelium targeting capability. In addition, absorption enhancers can further improve the oral absorption of essential oils. Nanoparticles modified with specific ligands, such as deoxycholic acid [27], cationic peptides [28], and lectins [29] are phagocytosed by intestinal epithelial cells through receptor-ligand interactions. Bile acids and their derivatives have been widely reported to promote the absorption of hydrophobic substances, macromolecules and nanoparticles, presumably due to the specific recognition of the apical sodium-dependent bile acid transporter (ASBT) by the ileum brush boundary [30,31]. Therefore, the insertion of bile acids in the nanoemulsion droplets is a potential strategy to further promote the oral absorption of essential oils.

Previously, the essential oil from *Alpinia zerumbet* Fructus (EOFAZ) has been confirmed with preventive effects on high glucose (HG)-induced endothelial injury [32–35]. The mechanisms may be correlated with the block of the nuclear factor kappa-B (NF-κB) signaling pathway and the up-regulation of nuclear factor-erythroid 2 related factor 2 (Nrf2), which relieves the inflammation response and oxidative stress [32,34,36]. The poor water solubility and instability of EOFAZ limit its absorption through the gastrointestinal tract (GIT). A high dosage was required in the treatment of HG-induced endothelial injury because of the low oral bioavailability [37–40]. The protein-dextran nanoemulsion has great potential to improve the oral bioavailability of EOFAZ, leading to enhanced protective effects on vascular endothelial injury (Scheme 1).

In this study, a protein-dextran emulsifier BD was synthesized by Maillard reaction was prepare an oral nanoemulsion with sodium deoxycholic acid (SD) inserted. Both fluorescein-loaded nanoemulsions (FL@BD_5/S) and EOFAZ-loaded nanoemulsions (EOFAZ@BD_5/S) were prepared by the microjet high-pressure homogenization method and optimized in terms of the physiochemical properties of nanoemulsions. The oral absorption of the process and mechanisms of FL@BD_5/S were investigated. The therapeutic effect of EOFAZ@BD_5/S on vascular endothelial injury was evaluated through *in vivo* and *in vitro* studies. This study shows the potential of nanoemulsion as a drug delivery platform for the treatment of vascular endothelial injury and provides a strategy for the development of novel traditional Chinese medicine preparations.

2. Methods

2.1. Preparation and characterization of fluorescein (FL)-loaded nanoemulsions

According to the research, BD_5, BD_{10} and BD_{20} were synthesized by the Maillard reaction [41]. In brief, BSA and DS (molecular weights 5 kDa, 10 kDa, 20 kDa) were dissolved in water at a molar ratio of 1:6. The pH of the solution was adjusted to 6, and then lyophilized. The lyophilized powder was reacted at 60 °C and 79 % humidity for 12, 24 and 36 h in order to obtain protein-polysaccharides BD_5, BD_{10} and BD_{20}.

Table 1
Parameters of FL nanoemulsions.

Nanoemulsions	Fls	Carrier materials	Concentration (mg/mL)
NR@BD/S	NR	BD and SD	0.4
DiR@BD/S	DiR	BD and SD	1
HIQ/NR@BD/S	HIQ/NR	BD and SD	HIQ of 1 and NR of 0.4

Subsequently, SD was dissolved in deionized water containing BD (10 mg/mL BSA) to obtain a water phase. The 1,1′-dioctadecyl-3,3,3′,3′-tetramethylindotricarbocyanine iodide (DiR), nile red (NR) or 3-hydroxyisoquinoline (HIQ)/NR were respectively mixed with medium chain triglyceride (MCT) to form an oil phase. The water phase and oil phase were mixed at the volume ratio of 4:1, followed by 5 min vortexing and 3 min ultrasonics at 65 W. Then, the primary emulsions were passed through a micro-jet high pressure homogenizer (NanoGenizer 20 K, Genizer LLC, Los Angeles, USA) at a pressure of 6000 psi for 3 cycles to obtain the nanoemulsion solutions loaded with FLs (Table 1). The nanoemulsions without DS or SD inserted were also prepared following the above procedures and denoted as FL@B and FL@BD. The loading efficiency (LE) of nanoemulsions was measured by fluorescence spectrophotometry (FS) (Method S3). The particle size, polydispersity index and zeta potential of nanoemulsions were measured by dynamic laser scattering (NanoBrook 90 Plus PALS, Brookhaven, US).

2.2. NR release profile from nanoemulsions in different simulated media

NR@B, NR@BD_5 or NR@BD_5/S were respectively mixed with simulated intestinal fluid (SIF) containing bile acids (Method S4), and then the mixtures were placed in a water bath thermostatic oscillator (37 ± 0.5 °C, 100 rpm/min). At the set time, the mixtures were gathered to determine the particle size and polydispersity index. The mixed solution was centrifuged at 3000 ×*g* for 5 min, and the supernatant was absorbed. Methanol was added to extract NR. The content of NR was determined by FS. The stability of nanoemulsions was analyzed by measuring the fluorescence energy transfer ratio (FR) (Method S5).

2.3. The transcellular permeability of nanoemulsions on Caco-2 monolayer cells

Caco-2 cells were seeded at a density of 5×10^4 cells per well on a polyester membrane of a transwell 24-well plate. A voltohmmeter (Millicell ERS-2, Millipore Co., Ltd., USA) was adopted for assessing the transepithelial electrical resistance (TEER) in Caco-2 cell monolayers. The TEER values reached at 500 Ω·cm^2 could be used in the following experiment. Free NR, NR@B, NR@BD_5, or NR@BD_5/S were added in the upper chambers, and PBS was added to the lower chambers. The TEER values were monitored at different incubation times. Samples were withdrawn from the lower chambers at 2 h to determine the NR content. Additionally, different inhibitors were added in the process of permeability experiments to investigate the transcellular mechanism of nanoemulsions (Method S6).

2.4. The distribution of DiR nanoemulsions in GIT

The C57BL/6 mice were fasted for 12 h before the experiment and randomly classified into 4 groups ($n = 3$). Free DiR, DiR@B, DiR@BD_5 and DiR@BD_5/S groups were administered by oral administration at DiR 0.7 mg/kg. At 0.5, 2, 6 and 12 h after administration, the mice were sacrificed and the GITs were dissected. The fluorescence images of the GITs were taken by an animal imaging system (IVIS Lumina III, Caliper, USA). The fluorescence intensities of the images were determined with Image J software (Image J 1.8.0, National Institutes of Health, USA).

2.5. Pharmacokinetic study of NR nanoemulsions

The C57BL/6 mice were randomly categorized into 4 groups ($n = 5$) and treated with free NR, NR@B, NR@BD_5 and NR@BD_5/S at 3 mg/kg NR *via* oral administration. Mice in each group were anesthetized at specified time points (0.25, 0.5, 1, 2, 4, 6, 12 and 24 h) using inhaled isoflurane with a small animal anesthetic equipment (ZS-MV-IV, Zhongshi Scientific Instruments Co., Ltd., Beijing, China). Blood samples were collected through the abdominal aorta and placed in heparinized tubes. After centrifugation at 1500 × *g* at 4 °C for 10 min, the plasma was collected. The plasma was mixed with methanol and centrifugated at 10000 ×*g* for 10 min. The content of NR in the supernatant was measured by FS. The plasma NR concentration was investigated by Win Nonlin 8.3 (Pharsight Corporation, Mountain View, US).

2.6. Cellular uptake of NR nanoemulsions

Human umbilical vein endothelial cells (HUVECs) were seeded in 96-well plates at a density of 5×10^3 cells/well for 12 h. Afterward, 100 μL of medium containing HG was added to a portion of the wells to induce an injury model of HUVECs. After being incubated for 24 h, the medium containing free NR, NR@B, NR@BD_5 and NR@BD_5/S (10 μg/mL NR) was added and incubated for 1 and 2 h, respectively. After co-incubation, the HUVECs were rinsed with cold PBS and fixed by immunostaining fixative for 30 min. Hoechst 33342 was added to stain the nucleus for 30 min. Images of each sample were collected by an operetta CLS high content imaging system (PerkinElmer, Berlin, Germany) at excitation/emission (Ex/Em) of 346/460 nm (Hoechst 33342) and 535/630 nm (NR).

2.7. The distribution of NR nanoemulsions in vivo

The study was carried out on type 2 diabetes mellitus (T_2DM) mice. The C57BL/6 mice were fed a high-fat and high-sugar diet (HFG) (containing 60 % fat, 20 % carbohydrate and 20 % protein) for 8 weeks and then injected with streptozotocin (STZ) 50 mg/kg for 3 days in order to obtain the T_2DM mouse model. For the T_2DM mice, free NR, NR@B, NR@BD_5 and NR@BD_5/S were oral administration at a dose of 3 mg/kg NR. The aorta, heart, liver, spleen, lung and kidney were collected and weighed. Subsequently, the organs were homogenized in PBS proportionally. After centrifugation at a low temperature, the supernatant of homogenate was mixed with methanol and vortexed. The obtained solutions were centrifuged at 10000 ×*g* at 4 °C for 10 min. The content of NR in the supernatant was measured by FS.

2.8. Preparation and characterization of EOFAZ encapsulated nanoemulsions

The BD_5 was synthesized and optimized to prepare EOFAZ nanoemulsions. Then, SD was added to the deionized water containing BD_5. EOFAZ was mixed with MCT at a concentration of 100 mg/mL EOFAZ. Then, 4 mL of BD_5/S mixture solution was mixed with 1 mL of the EOFAZ/MCT solution. The resultant solution was vortexed for 3 min and followed with ultrasonics, aiming to obtain a primary emulsion. Next, the primary emulsion was homogenized by a micro-jet high pressure homogenizer at a pressure of 6000 psi for 3 cycles and supplemented with deionized water to obtain the EOFAZ@BD_5/S. Additionally, the nanoemulsions without DS or SD inserted were also prepared and denoted as EOFAZ@B and EOFAZ@BD_5. Dynamic laser scattering was used to measure particle size, polydispersity index and zeta potential of the nanoemulsions. The morphology of EOFAZ nanoemulsions was observed using transmission electron microscopy (TEM, H-7800, Hitachi Co., Ltd., Japan) at an acceleration voltage of 100 kV. For the content detection of EOFAZ in the nanoemulsion, an ultraviolet spectrophotometry method was established (Fig. S5) with good precision and recovery (Table S3 and S4). The LE and loading capacity (LC) of EOFAZ

were determined by ultraviolet spectrophotometry (UV, 2700, Shimadzu, Japan) at 232 nm. LE (%) and LC (%) of EOFAZ are calculated based on formulas (1) and (2).

$$\text{LE}\ (\%) = \frac{\text{weight of loaded EOFAZ}}{\text{weight of initially added EOFAZ}} \times 100 \quad (1)$$

$$\text{LC}\ (\%) = \frac{\text{weight of loaded EOFAZ}}{\text{total weight of nanoemulsion}} \times 100 \quad (2)$$

2.9. The protection effect of EOFAZ nanoemulsions on injured HUVECs

2.9.1. Detection of cell viability

HUVECs were seeded in 96-well plates at a density of 5×10^3 cells/well. HUVECs were incubated with free EOFAZ (denoted as free EOFAZ group), EOFAZ@B, EOFAZ@BD_5 and EOFAZ@BD_5/S for 1 h before being exposed to the HG environment (35 mM) for 24 h. Cell viability was evaluated by both the trypan blue method and cell counting kit-8 (CCK-8) activity. After trypan blue dye addition, dead (stained) and viable (unstained) cells were counted. In the CCK-8 assay, We removed the medium and added 100 μL of 10 % CCK-8. After being incubated incubation for 1 h at 37 °C, the optical density (OD) of each well was measured at 450 nm using a microplate reader (LINDY BESSETTE BOX 998, BioTek Instruments, USA), with the blank medium as control. According to formula (3), the cell viability (%) was calculated.

$$\text{Cell viability}\ (\%) = \frac{\text{OD}_{\text{sample}} - \text{OD}_{\text{control}}}{\text{OD}_{\text{normal}} - \text{OD}_{\text{control}}} \times 100 \quad (3)$$

2.9.2. Detection of cell migration and tube formation

To assay the inhibitory effect of EOFAZ and EOFAZ nanoemulsions on inhibiting endothelial cell wound repair after mechanical injury of HUVECs. HUVECs were incubated with free EOFAZ, EOFAZ@B, EOFAZ@BD_5 and EOFAZ@BD_5/S for 1 h before scratched by 200 μL pipette tips. Then ECM medium (containing 35 mM HG) was added the scratched monolayer cell area. Images were acquired by a digital camera (Nikon, Japan) after 0 and 24 h. The migrated cells were quantified by Image J software.

According to the manufacturer's instructions, frozen BD Matrigel™ (Growth Factor Reduced, #356231) was melted into liquid at −4 °C. Matrigel and ECM basic medium were mixed and then incubated at 37 °C in 5 % CO_2 for 45 min. After the HUVECs were incubated with free EOFAZ, EOFAZ@B, EOFAZ@BD_5 and EOFAZ@BD_5/S for 1 h before being exposed to the HG environment (35 mM) for 24 h, the cells were seeded onto the Matrigel-coated plate and incubated with culture medium. The cultured after 24 h, a microscope was used to evaluate tube formation. Image J software was used to determine the number of tubes.

2.9.3. Reactive oxygen species (ROS) detection

Intracellular ROS accumulation was measured using Dichlorofluorescin diacetate (DCFH-DA, Invitrogen) reaction. Briefly, HUVECs were cultured with free EOFAZ, EOFAZ@B, EOFAZ@BD_5 and EOFAZ@BD_5/S for 24 h. Then the cells were washed and replenished with DCFH-DA (10 μM) in PBS for 30 min at 37 °C in dark. The cells were then trypsinized and resuspended in 1 mL PBS. Flow cytometry data were plotted and quantified based on the mean fluorescence intensity by using the Flow Jo software (Beckman, Indy, USA).

2.9.4. Western blot

HUVECs were incubated with free EOFAZ, EOFAZ@B, EOFAZ@BD_5 and EOFAZ@BD_5/S for 1 h before being exposed to the HG environment (35 mM) for 24 h. Cells were gathered and then lysed in RIPA lysis solution containing 100 mmol/L PMSF. The cell lysates were clarified by centrifugation at 12,000 ×*g* for 10 min at 4 °C. Protein concentrations in cell supernatants were quantified by adopting a BCA protein assay kit (Beyotime, Institute of Biotechnology, Jiangsu, China). Equal amounts (20 μg) of protein in each group were segregated by 10 % sodium dodecyl sulfate-polyacrylamide gel electrophoresis (SDS-PAGE) and electrotransferred to polyvinylidene fluoride (PVDF) membranes (Millipore, MA, USA). Subsequently, membranes were blocked with 5 % BSA (Solarbio, Beijing, China) at room temperature for 1.5 h and incubated overnight at 4 °C with Nrf2/NFE2L2 rabbit polyclonal antibody (1:1000 dilution), NF-κB p65 rabbit monoclonal antibody (1:1000 dilution) and GAPDH mouse monoclonal antibody (1:10000 dilution). After washing, membranes were incubated with secondary antibodies for 1.5 h at room temperature, and later visualized with an enhanced chemiluminescence (ECL) kit. A Syngene Gel Imaging System (ChemiDoc XRS + system, Bio Rad, USA) was employed to capture digital images of blots, which were then analyzed using Image Lab Software (Bio-Rad, USA).

For tissue samples, RIPA lysis solution containing 100 mmol/L PMSF was used to lyse the thoracic aortas of mice. Then total proteins were extracted and measured using a BCA protein assay kit. Protein lysates were exposed to 10 % SDS-PAGE and transferred to PVDF membranes. Subsequently, membranes were blocked with 5 % BSA before being treated with primary antibodies. Membranes were then cleaned and exposed to secondary antibodies. Next, the Nrf2 and NF-κB p65 protein bands were visualized and examined.

2.9.5. Detection of intracellular biochemical cytokines

Following a 24-h treatment period, supernatants from treated HUVECs of free EOFAZ, EOFAZ@B, EOFAZ@BD_5 and EOFAZ@BD_5/S groups were tested for SOD, GSH, MDA (Nanjing Jiancheng Bioengineering Institute, Nanjing, China), IL-1β, IL-6 and TNF-α (ZCIBIO, Shanghai, China) using commercially available kits.

2.10. The treatment of endothelial injury by EOFAZ nanoemulsions in T_2DM mice

2.10.1. Animal grouping and treatment of T_2DM mice model

C57BL/6 mice were randomized into 6 groups ($n = 7$): control, model, free EOFAZ, EOFAZ@B, EOFAZ@BD_5 and EOFAZ@BD_5/S. Mice in the control group were fed with water and standard rodent feed. Mice in the other five groups were fed with the HFG for 8 weeks and finally injected with 50 mg/kg STZ for 3 consecutive days. The successful establishment of the T_2DM mouse model was evaluated by body weight, fasting blood glucose (FBG) level, oral glucose tolerance test (OGTT), insulin tolerance test (ITT) and homeostasis model assessment of insulin resistance (HOMA-IR). The initial injury of the thoracic aorta was detected by hematoxylin-eosin (H&E) staining. All the EOFAZ formulation groups were subject to treatment at a dose of EOFAZ 60 mg/kg. Both the control and model groups were treated with the same volume of saline. During the whole period of the experiment, the body weights of mice were recorded every week. After 8 weeks, all mice were sacrificed, and blood and thoracic aortas were collected for analysis.

2.10.2. H&E staining

The thoracic aortas of mice were embedded in paraffin after being fixed in 10 % formalin. The samples (thoracic aortas and tissues) were cut into 5 μm slices and stained with H&E for optical microscopy analysis of vascular lesions and anomalies.

2.10.3. Detection of intracellular biochemical cytokines

Using kits as directed by the manufacturer, SOD, GSH, MDA, IL-1β, IL-6 and TNF-α levels in mice serum after treatment were measured. The absorbance was detected by a microplate reader at 450 nm.

2.10.4. Safety evaluation

Blood from the mice was added into a disposable vacuum heparin tube (Jiangxi Hongda Medical Equipment Group Co., Ltd., Jiangxi, China) and analyzed by a fully automatic blood cell analyzer (CAL 8000, Shenzhen Mindray Bio-Medical Electronic Co., Ltd., Shenzhen, China). The harvested tissues (heart, liver, spleen, lung and kidney) were immersed in a 10 % paraformaldehyde solution, followed by paraffin

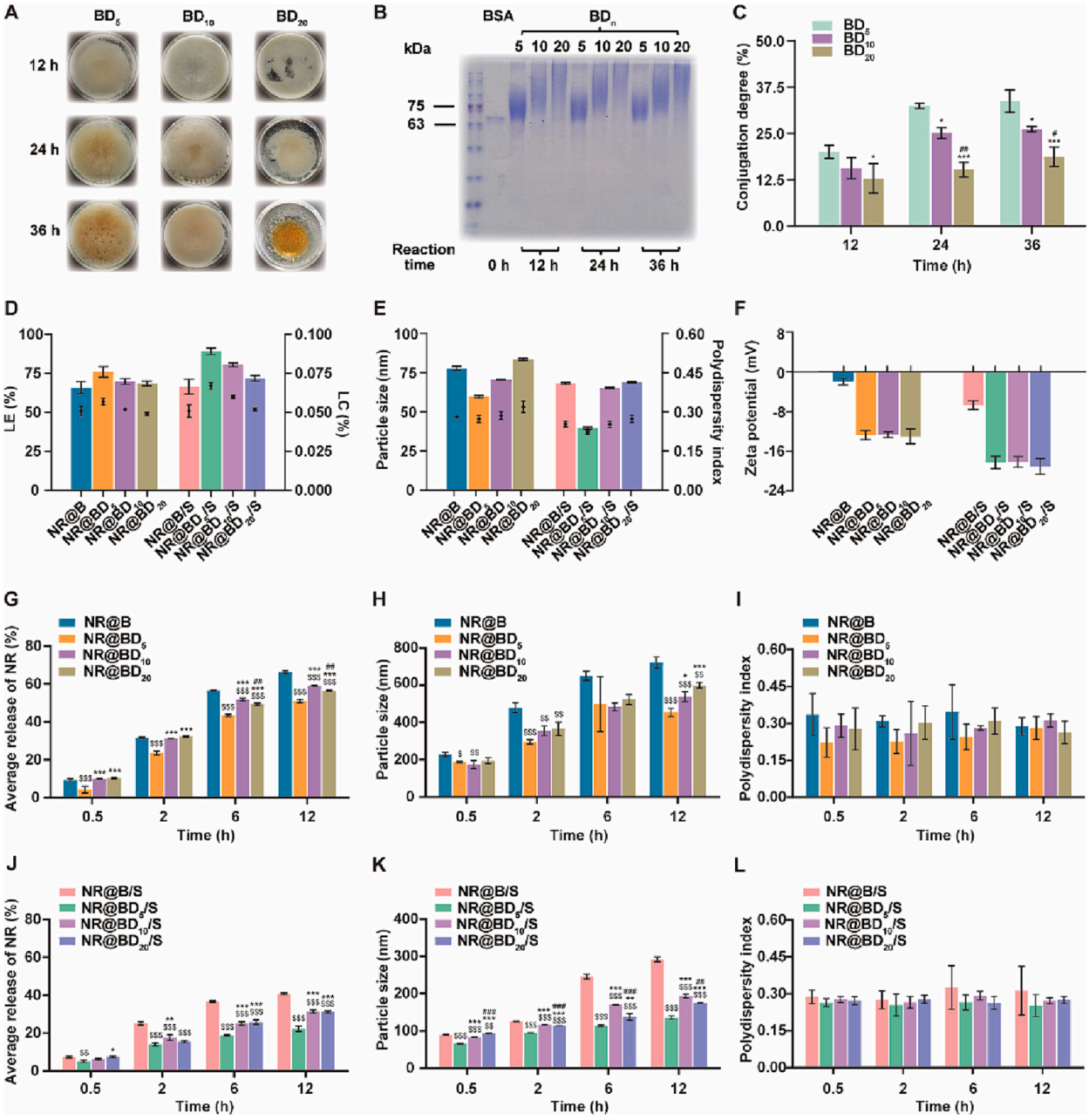

Fig. 1. Characterizations of NR nanoemulsions. (A) The appearance of BD_n materials with different reaction times (the material was taken out at different reaction time points and photographed). (B) SDS-PAGE of the various components. Marker and BSA (1–2 tracks from left to right), BD_5, BD_{10} and BD_{20} (3–11 tracks from left to right) with different reaction times. (C) The OPA method was used to detect the reaction percentage of the amino group of BSA and the carbonyl group of DS. $^{*}p < 0.05$, $^{**}p < 0.01$ and $^{***}p < 0.001$ relative to BD_5, $^{\#}p < 0.05$, $^{\#\#}p < 0.01$ and $^{\#\#\#}p < 0.001$ relative to BD_{10}. (D) The inclusion encapsulation efficiency of NR (LE-bars and LC-dots), (E) particle size (bars) and polydispersity index (dots), (F) zeta potential in different nanoemulsions. (G and J) The release of NR, (H and K) particle size and (I and L) polydispersity index of nanoemulsions after 12 h in SIF (containing bile acid) at 37 °C. (G, H and I) $^{\$}p < 0.05$, $^{\$\$}p < 0.01$ and $^{\$\$\$}p < 0.001$ relative to NR@B, $^{*}p < 0.05$, $^{**}p < 0.01$ and $^{***}p < 0.001$ relative to NR@BD_5, $^{\#}p < 0.05$, $^{\#\#}p < 0.01$ and $^{\#\#\#}p < 0.001$ relative to NR@BD_{10}. (J, K and L) $^{\$}p < 0.05$, $^{\$\$}p < 0.01$ and $^{\$\$\$}p < 0.001$ relative to NR@B/S, $^{*}p < 0.05$, $^{**}p < 0.01$ and $^{***}p < 0.001$ relative to NR@BD_5/S, $^{\#}p < 0.05$, $^{\#\#}p < 0.01$ and $^{\#\#\#}p < 0.001$ relative to NR@BD_{10}/S. Data are shown as mean ± SD ($n = 3$).

embedding for H&E staining.

2.11. Statistical analysis

The mean standard deviation (mean ± SD) was used to express all experimental data. The data were processed using GraphPad Prism 8 (La Jolla, CA). The one-way ANOVA followed by the post-hoc Tukey test was used to detect the statistical significance among groups. $^{*}p < 0.05$, $^{**}p < 0.01$ and $^{***}p < 0.001$ were considered to be of statistical significance.

3. Results and discussion

3.1. Preparation and optimization of nanoemulsions

The Maillard reaction involves a series of non-enzymatic reactions between the free amino groups of proteins and the carbonyl groups of reducing carbohydrates, which is one of the synthesis methods for

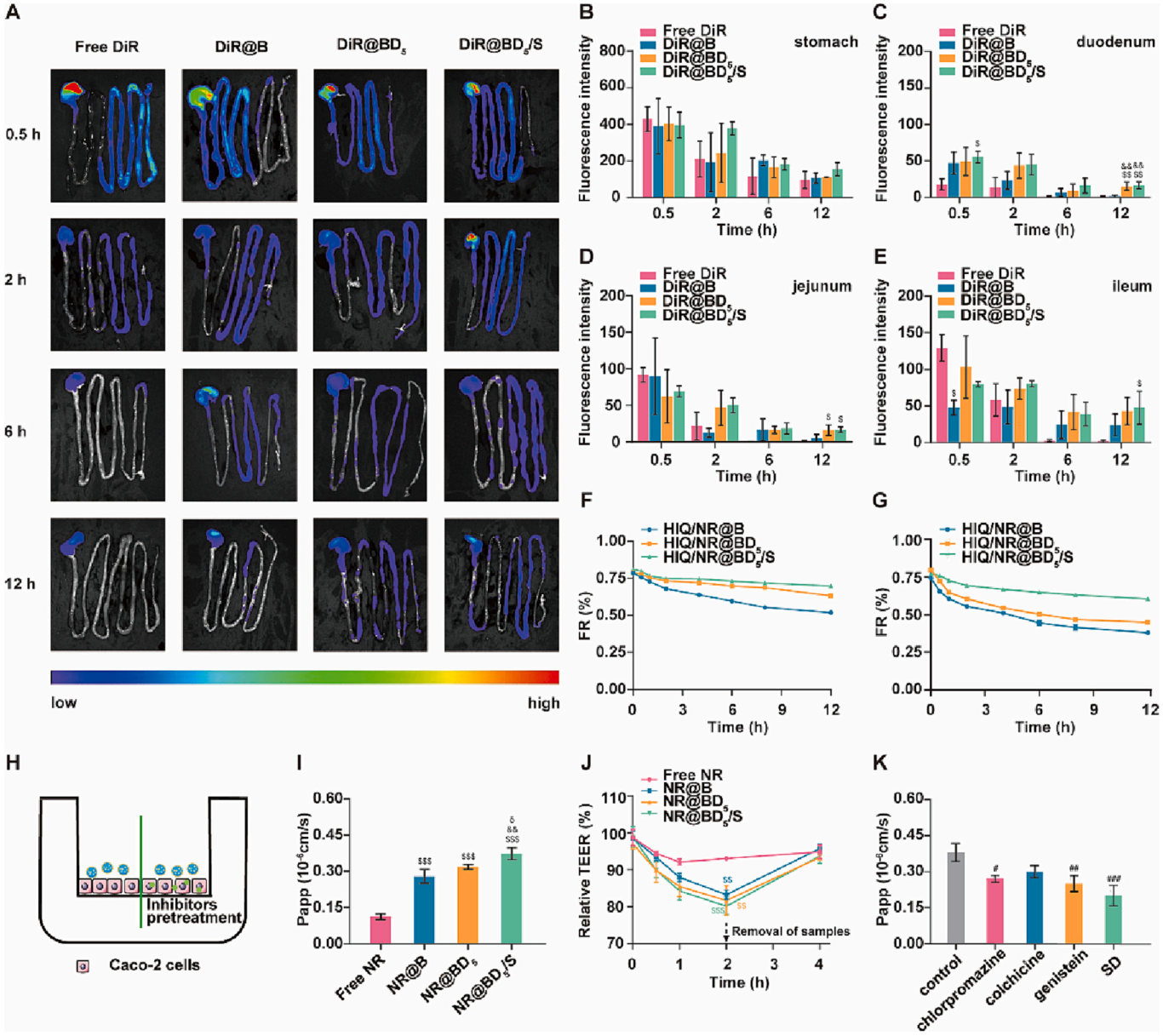

Fig. 2. (A) Representative fluorescence images of the GITs of the mice excised at 0.5, 2, 6 and 12 h after oral administration with free DiR and DiR nanoemulsions. The fluorescence intensities of (B) stomach, (C) duodenum, (D) jejunum and (E) ileum of the mice after the oral administration. $^{\$}p < 0.05$, $^{\$\$}p < 0.01$ and $^{\$\$\$}p < 0.001$ relative to free DiR, $^{\&}p < 0.05$, $^{\&\&}p < 0.01$ and $^{\&\&\&}p < 0.001$ relative to DiR@B, $^{\delta}p < 0.05$, $^{\delta\delta}p < 0.01$ and $^{\delta\delta\delta}p < 0.001$ relative to DiR@BD_5. FRET intensity of nanoemulsions prepared with HIQ and NR after incubation in (F) SGF and (G) SIF for different times. The residual fluorescent intensity represented the structural integrity of nanoemulsions. (H) Schematic illustration of the transwell Caco-2 cell monolayer experiment. (I) P_{app} values of free NR and NR nanoemulsions in Caco-2 cell monolayers. (J) Relative TEER changes of the Caco-2 cell monolayers in different groups. $^{\$}p < 0.05$, $^{\$\$}p < 0.01$ and $^{\$\$\$}p < 0.001$ relative to free NR, $^{\&}p < 0.05$, $^{\&\&}p < 0.01$ and $^{\&\&\&}p < 0.001$ relative to NR@B, $^{\delta}p < 0.05$, $^{\delta\delta}p < 0.01$ and $^{\delta\delta\delta}p < 0.001$ relative to NR@BD_5. The nanoemulsions were permeated from the Caco-2 cell monolayers after 2 h incubation. (K) P_{app} values of the NR@BD_5/S in Caco-2 cell monolayers treated with various inhibitors. $^{\#}p < 0.05$, $^{\#\#}p < 0.01$ and $^{\#\#\#}p < 0.001$ relative to control. Data are shown as mean ± SD ($n = 3$).

protein glycosylation [42]. In this study, the free amine groups on BSA and the reduced carbonyl groups on DS through irreversible rearrangement to generate the covalently conjugates. The glycosylation degree of proteins is influenced by reaction conditions, of which reaction time is the most important. As the Maillard reaction does not have significant discoloration at the initial stage, yellow or brown products are produced at the intermediate or final stages of the reaction. Therefore, we optimized the reaction time and limited the reaction to the initial stage to avoid the formation of by-products. DS of different molecular weights were used to obtain a series of BD grafts by controlling the reaction time (12, 24 and 36 h). Fig. 1A displays the appearance of BD. The graft showed an obvious colour change after 24 h reaction, suggesting that it was beyond the primary stage. The SDS-PAGE results confirmed that DS was covalently attached to BSA and a larger molecular weight of conjugates was generated (Fig. 1B). The grafting rates of BD prepared above were measured by the *o*-phenylenedicarboxaldehyde (OPA) method (Fig. 1C). The results demonstrated that the grafting rate of the DS gradually increased with time. Furthermore, the grafting rate of DS decreased with the increased molecular weight. It might be correlated with the length of the DS chain, which impeded the reaction between BSA and DS through spatial resistance. By contrast, smaller molecular weight (5 kDa) DS is easier to conjugate with BSA to obtain BD_5 and form short and dense hydrophilic shell layers on the emulsion droplets.

A

Pharmacokinetic parameters of the NR-loaded formulations after a single oral administration to mice plasma (mean ± SD, n = 5).

Pharmacokinetic parameters	Free NR	NR@B	NR@BD_5	NR@BD_5/S
$T_{1/2}$ (h)	2.67 ± 0.41	3.85 ± 0.75	4.34 ± 0.84	6.28 ± 3.22$^{\$}$
T_{max} (h)	0.60 ± 0.22	1.00 ± 0.00	1.00 ± 0.00	1.40 ± 0.55$^{\$\$}$
C_{max} (ng/mL)	105.68 ± 5.26	147.25 ± 43.54	179.05 ± 25.04$^{\$\$}$	212.80 ± 34.09$^{\$\$\$,\&}$
AUC_{0-t} (h*ng/mL)	368.63 ± 39.5	529.09 ± 109.02	969.99 ± 164.56$^{\$\$\$,\&\&\&}$	1330.31 ± 182.11$^{\$\$\$,\&\&\&,\delta\delta}$
$AUC_{0-\infty}$ (h*ng/mL)	374.68 ± 35.87	542.53 ± 102.11	993.23 ± 168.83$^{\$\$\$,\&\&}$	1434.28 ± 220.72$^{\$\$\$,\&\&\&,\delta\delta}$
Cl/F (mL/h/kg)	8069.36 ± 817.15	5681.32 ± 1009.86$^{\$\$\$}$	3108.62 ± 651.33$^{\$\$\$,\&\&\&}$	2135.18 ± 357.47$^{\$\$\$,\&\&\&}$
MRT (h)	3.18 ± 0.27	4.44 ± 0.83	5.20 ± 0.96$^{\$\$}$	6.00 ± 0.70$^{\$\$\$,\&}$

$\$p$ vs Free NR, $\&p$ vs NR@B, δp vs NR@BD_5

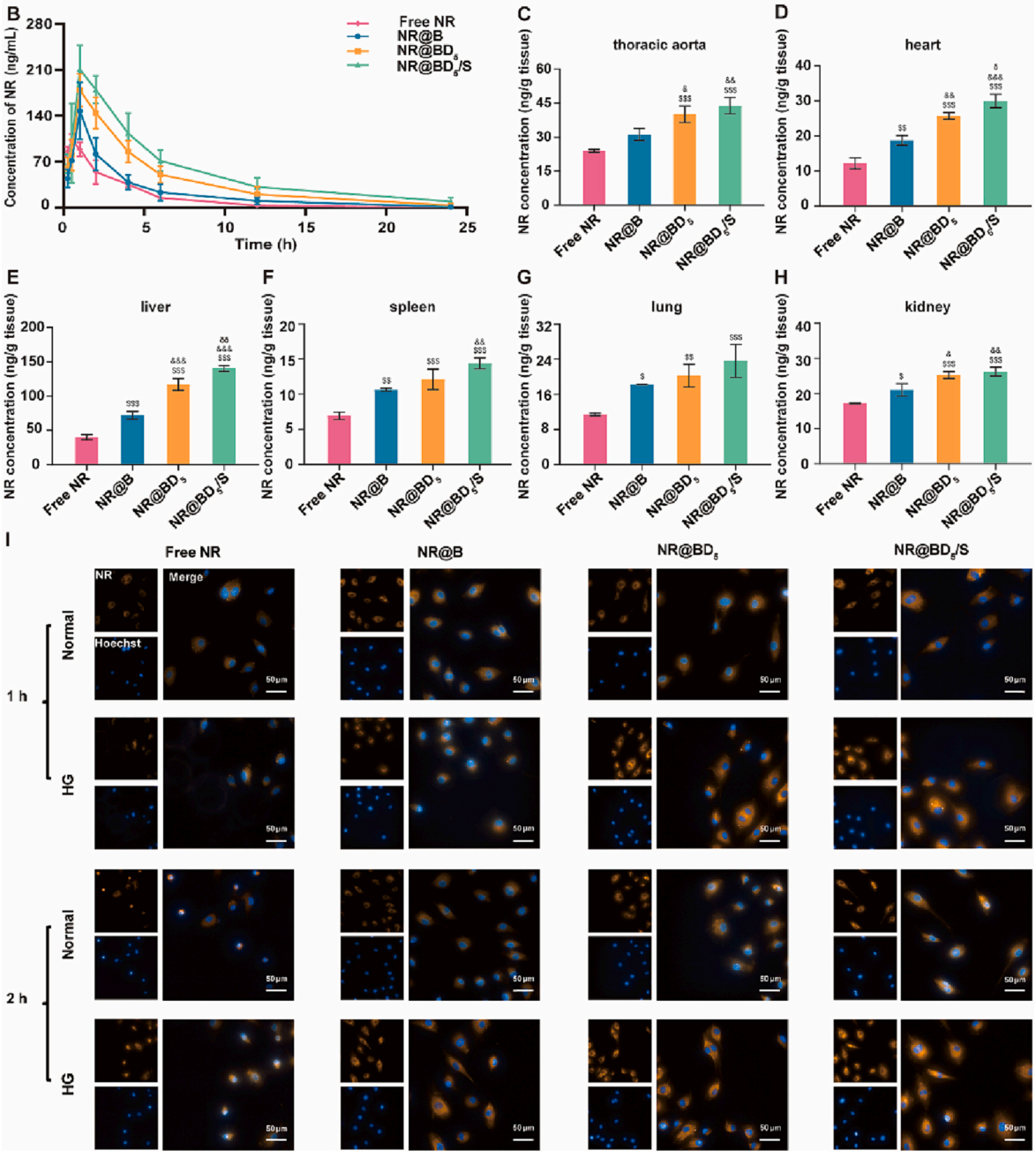

Fig. 3. (A) The pharmacokinetic parameters and (B) drug concentration-time curves of free NR and NR nanoemulsions at a dose of 3 mg/kg in mice after oral administration ($n = 5$). The distribution of NR in T_2DM mice at (C) thoracic aorta, (D) heart, (E) liver, (F) spleen, (G) lung and (H) kidney after oral administration of free NR and NR nanoemulsions at a dose of 3 mg/kg for 12 h. $^{\$}p < 0.05$, $^{\$\$}p < 0.01$ and $^{\$\$\$}p < 0.001$ relative to free NR, $^{\&}p < 0.05$, $^{\&\&}p < 0.01$ and $^{\&\&\&}p < 0.001$ relative to NR@B, $^{\delta}p < 0.05$, $^{\delta\delta}p < 0.01$ and $^{\delta\delta\delta}p < 0.001$ relatives to NR@BD_5. Data were shown as mean ± SD ($n = 3$). (I) *In vitro* cellular uptake. Operetta CLS high content imaging system of the intracellular distribution of free NR, NR@B, NR@BD_5 and NR@BD_5/S in normal or HG for HUVECs after 1 and 2 h incubation (scale bar 50 μm).

NR was loaded for *in vitro* and *in vivo* fluorescence tracking of the nanoemulsions (Fig. 1D-F). Compared with @B, @BD exhibited no significant changes in drug LE, LC, particle size, or particle size distribution, while the modification of negatively charged DS resulted in a significant decrease in zeta potential. DS modification may hinder the interaction of the nanoemulsion with the intestinal epithelial cells (IECs) membrane due to its negative charge, causing poor epithelial cell transport. Therefore, we incorporated a certain percentage of bile salt-SD on the nanoemulsion surface to improve the IECs' transport. It was found that the admixture of SD has no significant effect on the basic physicochemical characteristics of the nanoemulsion.

Following oral administration, the drug-loaded nanoemulsion should be able to withstand the destruction of various enzymes and endogenous bile salts in the GIT, and overcome the gastrointestinal barrier to transport through the digestive tract [43,44]. Particularly, the effect of intestinal fluid containing endogenous bile salts on the structure of the emulsion droplets should not be neglected. We studied the stability of NR-loaded nanoemulsions in SIF containing bile salt. After 12 h of incubation, NR@B showed 66.34 ± 0.61 % cumulative release, while protein-polysaccharide nanoemulsions exhibited lower cumulative release of NR, especially for NR@BD_5 (Fig. 1G). It was indicated that proteins can be enzymatically cleaved to peptides after digestion, and most of the polysaccharides were able to retard the release rate and reduce the protein cleavage percentages, maintaining the structural integrity of the nanoemulsion. However, the particle size in the SIF increased to over 400 nm after 12 h, even for @BD (Fig. 1H, I). Surprisingly, the insertion of SD exhibited better integrity of the nanoemulsion in SIF (Fig. 1J–L). After incubation for 12 h, NR@BD_5/S showed 22.23 ± 1.38 % cumulative release of NR, and the particle size increased slightly to 135.61 ± 4.40 nm. Since bile salts play important roles in the absorption of fat, they are supposed to be inserted into the oil phase of nanoemulsions during incubation, resulting in the incorporation of emulsion droplets. Enlightened by the function of bile salts, SD was involved in the preparation of nanoemulsions to prevent further insertion and destruction by the bile salts in the medium. According to the results, the SD-involved nanoemulsions slightly increased as the incubation time lasted. It is speculated that the ordered arrangement of SD and BD constitutes the @BD, which is much more stable than the disordered arrangement formed by the uncontrolled insertion of bile salts into the nanoemulsion. Therefore, an appropriate ratio of SD inserted into the surface of @BD is a good strategy that can be used to resist the destruction of endogenous bile salts that further enhance the stability of EOFAZ nanoemulsions in GIT. Based on the above-mentioned results, BD and SD were used to prepare nanoemulsions in subsequent studies.

3.2. Effect of oral absorption of FL-loaded nanoemulsions

Above all, the properties and LE/LC of fluorescence-loaded nanoemulsions were characterized (Fig. S1–3). Free DiR, DiR@B, DiR@BD_5 and DiR@BD_5/S were orally administered to mice, respectively. The gastrointestinal organs of the mice were removed at different time points and fluorescence signals were detected. As displayed in Fig. 2A–E, the retention time of DiR@BD_5/S in the stomach was longer than that of DiR@B and DiR@BD_5. All of the nanoemulsions were higher than that of free DiR. After 2 h of administration, the overall fluorescence intensity in the small intestine of the nanoemulsions groups was higher than that of free DiR group, especially for DiR@BD_5 group. Combined with the results of the FRET study (Fig. 2F, G), this may be caused by the longer maintenance of the intact form of DiR@BD_5/S in the gastric and intestinal fluid and its better stability during gastrointestinal transport, causing the retention of fluorescence in the stomach and small intestine. Particularly, the overall fluorescence intensity of the DiR@BD_5/S group in the ileum was significantly higher than that of free DiR group at 12 h (Fig. 2E). It might be attributed to SD-mediated retention of DiR@BD_5/S in the ileum and ASBT receptors mediating cellular uptake of IECs.

IECs are the main barriers that limit the penetration and absorption of oral drugs through the GIT [45,46]. In this study, a single-layer model of Caco-2 cells was used to simulate the intestinal absorption barrier. In order to evaluate the permeability of NR-loaded nanoemulsions across IECs, P_{app} values of NR *via* Caco-2 monolayer cells were calculated (Fig. 2H). As shown in Fig. 2I, in relative to free NR group, the P_{app} value of NR in NR nanoemulsion groups was around 2–3 times that of free NR group. Noteworthy, the NR@BD_5/S group consistently shows the optimum penetration effect. TEER is commonly used to predict the contribution of paracellular permeation to oral absorption [47]. As shown in Fig. 2J, TEER was immediately decreased in all nanoemulsions, in contrast to the constant value in the free NR group. Furthermore, the gradually increasing TEER after the removal of nanoemulsion indicated that the tight junctions had been restored. Therefore, we suggest that nanoemulsion can instantly and reversibly open the tight junctions of the Caco-2 monolayer, which is the main mechanism of paracellular permeation. Endocytosis provides an effective way of getting substances into cells through membrane phagocytosis, which is mainly divided into clathrin-mediated endocytosis, caveolin-mediated endocytosis and micropinocytosis [48,49]. The mechanisms by which the NR@BD_5/S group promotes penetration on the monolayer of Caco-2 cells were investigated (Fig. 2K). Chlorpromazine made a significant effect on the P_{app} value in the NR@BD_5/S group, indicating that clathrin-mediated endocytosis was involved in the transcellular transport of nanoemulsion. Colchicine can inhibit the polymerization of tubulin to lower membrane fluidity and inhibit cell micropinocytosis uptake [50]. The P_{app} value of the NR-loaded nanoemulsion slightly decreased after the addition of colchicine, implying that micropinocytosis was not the main transmembrane route of NR@BD_5/S. The P_{app} value of the NR@BD_5/S group decreased significantly after the addition of genistein, which indicated that caveolin-mediated endocytosis mainly contributed to the transport of nanoemulsions. Additionally, SD significantly reduced the P_{app} value of the NR@BD_5/S group. In summary, the transport of NR@BD_5/S *via* IECs mainly relied on the transcellular pathway and cellular bypass pathway, where the transcellular pathway was probably achieved through the clathrin, caveolin and ASBT.

3.3. Pharmacokinetic study on NR-loaded nanoemulsions

The plasma drug concentration-time curves of NR after oral administration of free NR, NR@B, NR@BD_5 and NR@BD_5/S are presented in Fig. 3B. The plasma drug concentration-time curves were processed by the software, and the pharmacokinetic parameters after non-atrioventricular fitting were shown in Fig. 3A. The area under the curve (AUC) of nanoemulsions increased significantly in relative to the free NR group. $AUC_{0-\infty}$ of the NR@B, NR@BD_5 and NR@BD_5/S groups were 1.45, 2.65 and 3.83 times greater than that of the free NR group, respectively. These results indicated that the NR nanoemulsions had higher oral bioavailability than the free NR. NR@BD_5/S showed improved C_{max}, AUC of NR *in vivo*, which could lay a good foundation for drug-carrying nanoemulsions to better exert their efficacy *in vivo*. In addition, MRT in the NR@B, NR@BD_5 and NR@BD_5/S groups were 1.40, 1.64 and 1.89 times longer than those in the free NR group. It indicated that the surface of NR@BD_5/S maintained hydrophilicity and electronegativity. This reduced the binding of opsonin in plasma and prolonged blood circulation time in order to target injured vascular endothelial cells *in vivo*.

3.4. The targeting efficacy of NR-loaded nanoemulsions

The biodistribution of nanoemulsions in T_2DM mice was further investigated. NR concentrations in the major organs (thoracic aorta, heart, liver, spleen, lung and kidney) were measured 12 h after oral administration. The tissue concentrations of the NR nanoemulsions were higher in each organ than in the free NR group (Fig. 3C–H). Compared with the NR nanoemulsions, free NR showed the lowest accumulation in

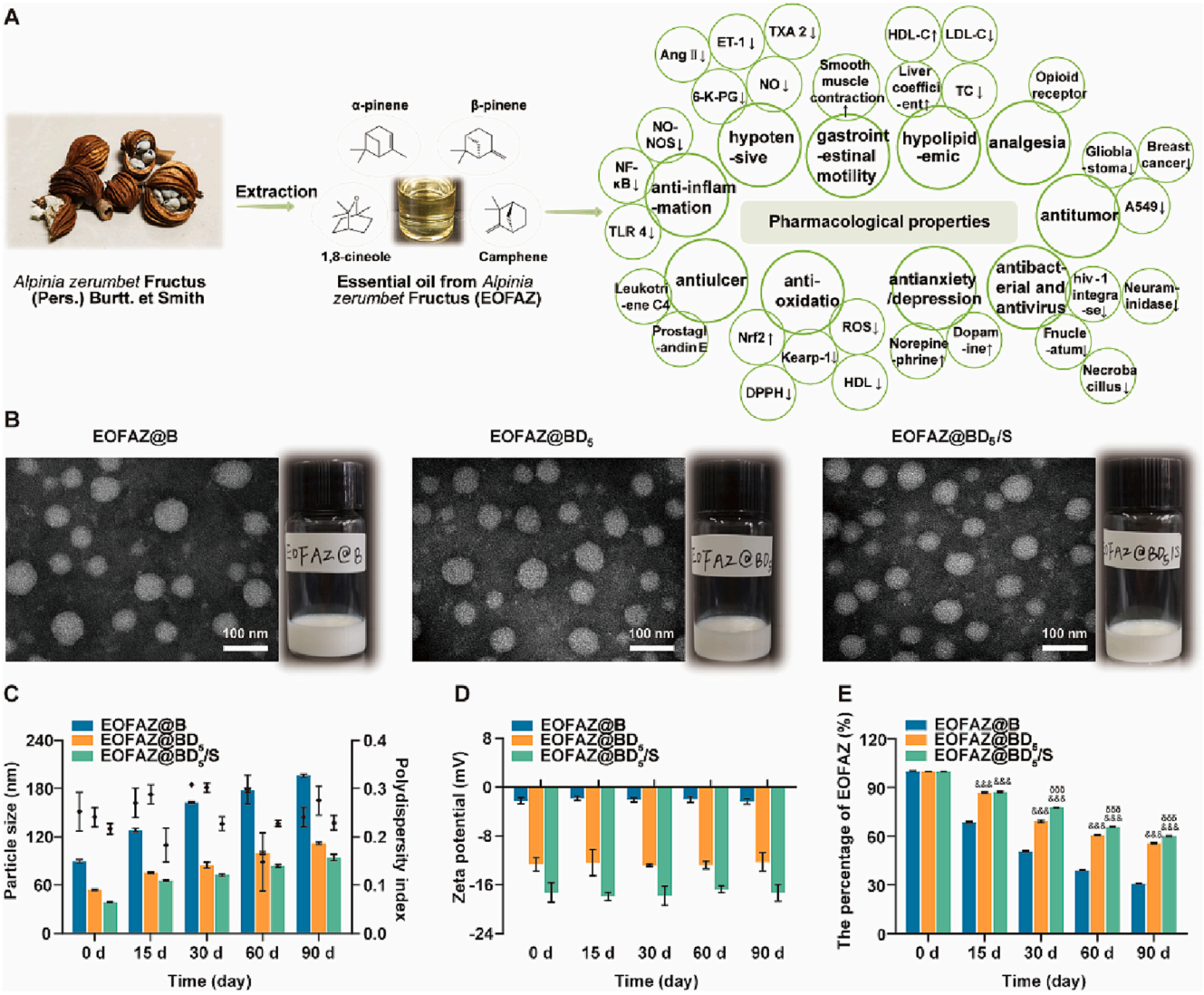

Fig. 4. Characterization of EOFAZ nanoemulsions. (A) Illustrative scheme with the most important bioactive constituents of essential oil from *Alpinia zerumbet* Fructus (EOFAZ) and pharmacological properties. (B) The representative TEM images and appearance of EOFAZ@B, EOFAZ@BD_5 and EOFAZ@BD_5/S (scale bar 100 nm). (C) The particle size (bars) and polydispersity index (dots), (D) zeta potential and (E) the percentage contents (compared with 0 d) of EOFAZ of nanoemulsions after 90 days at 4 °C. Data were shown as mean ± SD ($n = 3$). $^{\&}p < 0.05$, $^{\&\&}p < 0.01$ and $^{\&\&\&}p < 0.001$ relative to EOFAZ@B, $^{\delta}p < 0.05$, $^{\delta\delta}p < 0.01$ and $^{\delta\delta\delta}p < 0.001$ relative to EOFAZ@BD_5.

the main metabolic organs (liver and kidney). It was consistent with the longer MRT of NR nanoemulsions after oral administration. Notably, the cumulative concentrations of NR@BD_5 and NR@BD_5/S in the thoracic aorta were significantly higher than those of NR@B. Therefore, it was speculated that NR@B had low oral bioavailability and was not selective for injured vascular endothelium. It has been reported that the scavenger receptor CL-P1 is overexpressed on injured vascular endothelial cells, which is the targeting receptor of DS [26,51]. To confirm the targeting ability of DS modified nanoemulsions to injured vascular endothelial cells, an *in vitro* HG induced endothelial cell model established on HUVECs was constructed to investigate the distribution of NR nanoemulsions (Fig. 3I). The fluorescence intensities of the NR nanoemulsions were slightly higher than those of the free NR in normal HUVECs at different times, while there was no notable difference among the NR nanoemulsions. In HG-induced injured HUVECs, the fluorescence intensities of NR@BD_5 and NR@BD_5/S were significantly higher than those of the NR@B group. It is speculated that although CL-P1 expressed on the surface of injured HUVECs might promote the internalization of @BD, the specific mechanism remains unclear and needs further study.

3.5. The characterization of EOFAZ-loaded nanoemulsions

Alpinia zerumbet Fructus is the fresh or dried mature fruit of *Alpinia zerumbet* (Pers.) Burtt. et Smith [32]. The EOFAZ was extracted and identified based on our previous methods [52]. The main active components of the EOFAZ include α-pinene, camphene, 1,8-cineole and β-pinene [53,54]. GC–MS/MS chromatography was used to analyze the main components of EOFAZ (Method S6) [55,56]. By comparison with the database, four main components in EOFAZ and EOFAZ nanoemulsions were confirmed (Fig. S4) and the percentage of content were calculated (Table S2). EOFAZ shows a wide range of pharmacological activities, including anti-inflammatory, antioxidant, anti-ulcer, anti-anxiety/depression, anti-tumor, hypotensive, analgesic, *etc.* (Fig. 4A). As shown in Fig. 4B, EOFAZ nanoemulsions were characterized by TEM. It was shown that the emulsion droplets were all spherical. The nanoemulsion prepared with BD_5 instead of BSA, has smaller particle sizes, suggesting that BD_5 has a stronger emulsification ability and is beneficial for forming smaller emulsion droplets. The particle size of EOFAZ@B was 89.38 ± 2.06 nm, whereas EOFAZ@BD_5 and EOFAZ@BD_5/S decreased to 54.15 ± 0.75 nm and 38.90 ± 0.41 nm,

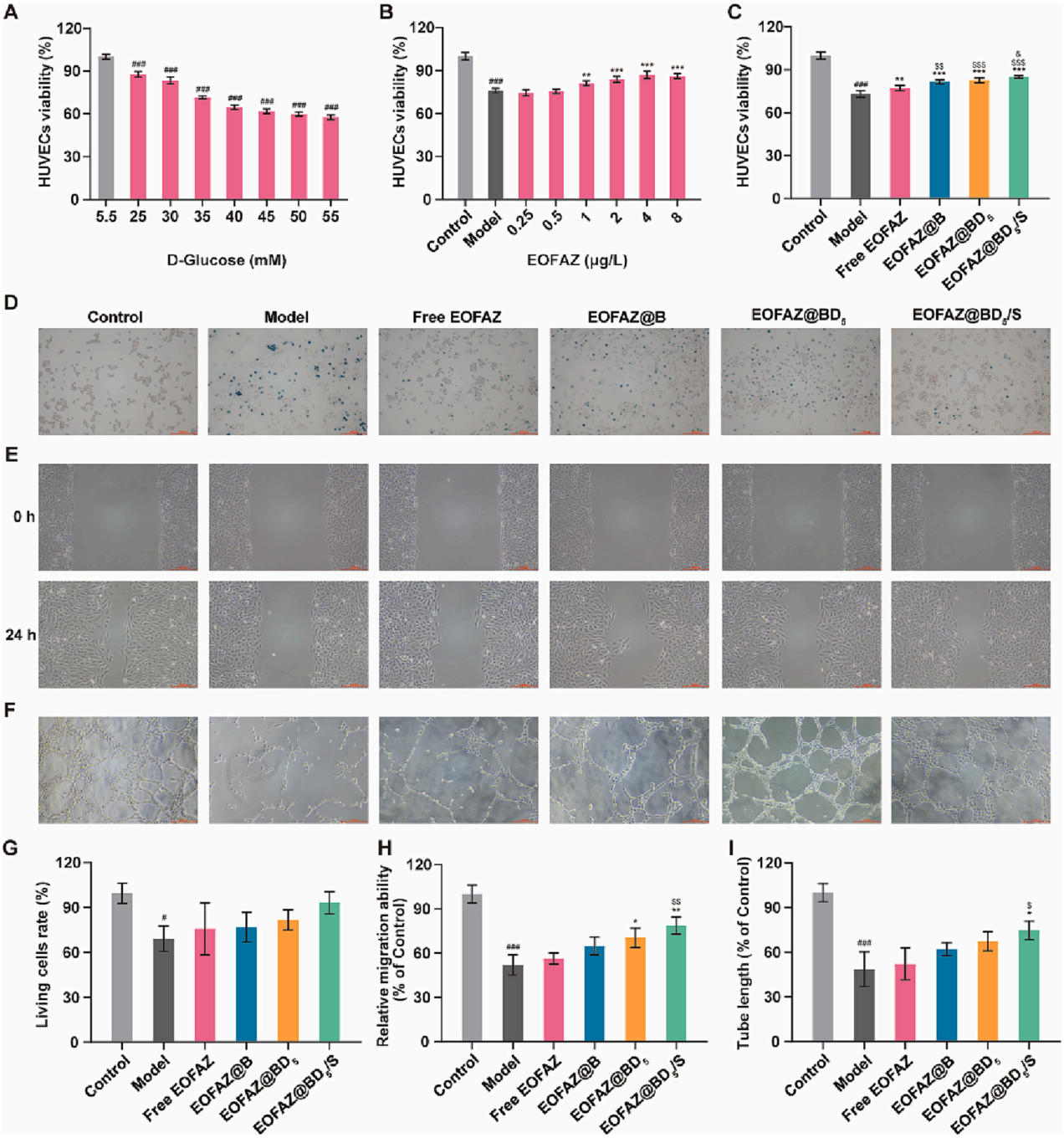

Fig. 5. Protective effects of the EOFAZ nanoemulsions on the viability and angiogenesis of HUVECs. Cell viability was assessed using a CCK-8 assay ($n = 6$). (A) The dose-effect of HG on HUVECs viability. HUVECs were pretreated with (B) different concentrations of EOFAZ and (C) EOFAZ nanoemulsions concentration was 1 μg/L of each nanoemulsion for 1 h, and then stimulate HUVECs with HG (35 mmol/L) for 24 h, and the cell viability was measured. (D and G) Trypan blue staining and counting, (E and H) cell migration assay and (F and I) tube formation assay were performed on HUVECs cells treated with HG (35 mmol/L) for 24 h (scale bar 200 μm). Data were shown as mean ± SD ($n = 3$). $^{\#}p < 0.05$, $^{\#\#}p < 0.01$ and $^{\#\#\#}p < 0.001$ relative to control, $^{*}p < 0.05$, $^{**}p < 0.01$ and $^{***}p < 0.001$ relative to model, $^{\$}p < 0.05$, $^{\$\$}p < 0.01$ and $^{\$\$\$}p < 0.001$ relative to free EOFAZ, $^{\&}p < 0.05$, $^{\&\&}p < 0.01$ and $^{\&\&\&}p < 0.001$ relative to EOFAZ@B, $^{\delta}p < 0.05$, $^{\delta\delta}p < 0.01$ and $^{\delta\delta\delta}p < 0.001$ relative to EOFAZ@BD_5.

respectively. After the insertion of negatively charged BD_5, the surface charge of the nanoemulsion changed from nearly neutral to negative (−12.68 ± 1.10 mV). After SD was involved, the zeta potential of nanoemulsions further decreased to −17.26 ± 1.62 mV, indicating that SD was presented on the surface of nanoemulsions. The LE of EOFAZ was higher than 71 % in all the nanoemulsions, and the modification of DS and SD made no effect on the drug encapsulation (Table S5). The emulsion is a thermodynamically unstable system that is prone to flocculation, coalescence, delamination and precipitation during storage. The variation of EOFAZ nanoemulsions concerning particle size, distribution, zeta potential and drug content at 4 °C was monitored to evaluate the stability. As shown in Fig. 4C, the particle size of EOFAZ@B increased by 100 nm after 90 days. Nevertheless, the nanoemulsion prepared with BD_5 showed only an increase of 60 nm on the 90th day. The insertion of SD further strengthened the stability of the EOFAZ@BD_5/S. In addition, no variation in zeta potential for all the

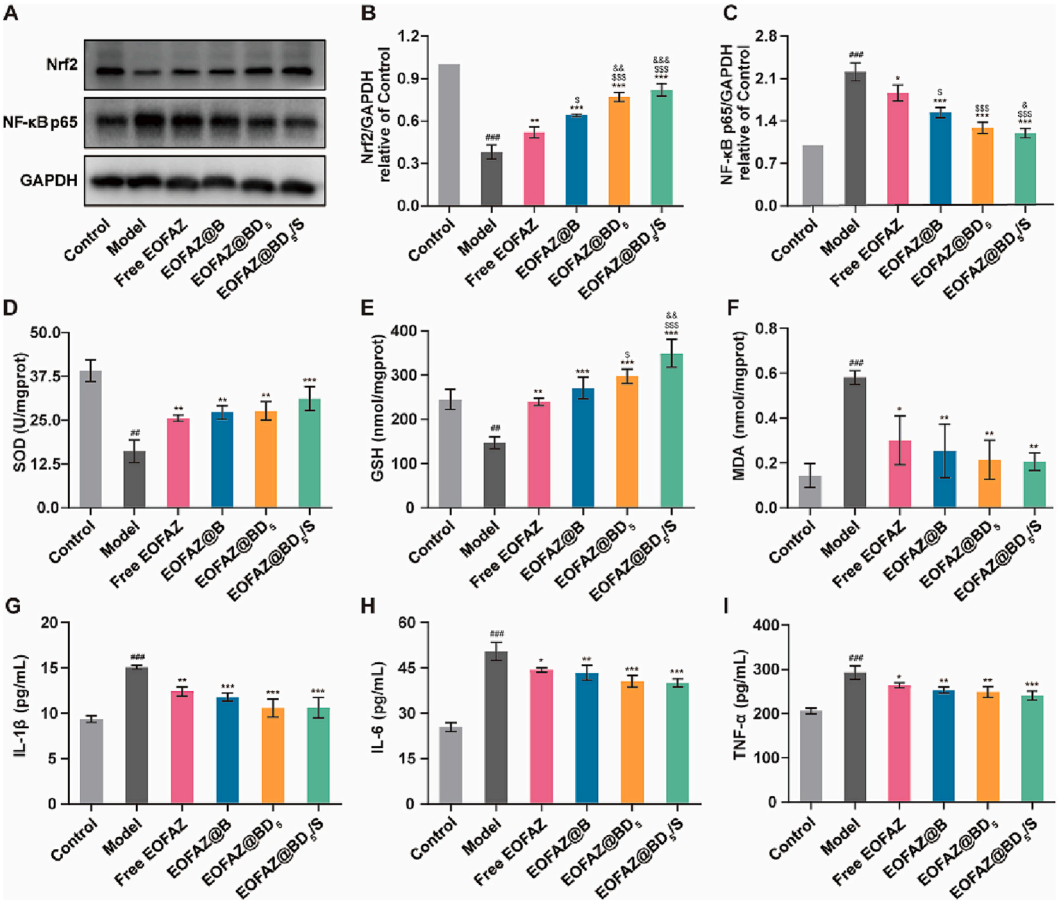

Fig. 6. Effects of the EOFAZ nanoemulsions on HG-induced injury of HUVECs. (A) The expression of Nrf2 and NF-κB p65 in HUVECs were detected by western blot and (B and C) quantitative analysis by densitometry. Expressed relative to GAPDH. The expression of (D) SOD, (E) GSH, (F) MDA, (G) IL-1β, (H) IL-6 and (I) TNF-α in culture supernatants of HUVECs were measured by kits. Data were shown as mean ± SD ($n = 3$). $^{\#}p < 0.05$, $^{\#\#}p < 0.01$ and $^{\#\#\#}p < 0.001$ relative to control, $^{*}p < 0.05$, $^{**}p < 0.01$ and $^{***}p < 0.001$ relative to model, $^{\$}p < 0.05$, $^{\$\$}p < 0.01$ and $^{\$\$\$}p < 0.001$ relative to free EOFAZ, $^{\&}p < 0.05$, $^{\&\&}p < 0.01$ and $^{\&\&\&}p < 0.001$ relative to EOFAZ@B, $^{\delta}p < 0.05$, $^{\delta\delta}p < 0.01$ and $^{\delta\delta\delta}p < 0.001$ relative to EOFAZ@BD$_5$.

nanoemulsions was shown after 90 days of storage (Fig. 4D). The decrease in repulsion force between nanoemulsion droplets, which leads to droplet merger, could be the primary cause of particle size increase. During storage, the content of EOFAZ in nanoemulsions was measured (Fig. 4E). On the 90th day, the content of EOFAZ decreased to 30.72 ± 0.18 %, while EOFAZ@BD$_5$ and EOFAZ@BD$_5$/S remained higher than 55 % of EOFAZ. Since the leakage of EOFAZ is closely related to the integrity of nanoemulsion droplets, EOFAZ@BD$_5$ and EOFAZ@BD$_5$/S exhibited better stability *in vitro*.

3.6. Protection effects of EOFAZ-loaded nanoemulsions in vitro

To further explore the protective effect of EOFAZ-loaded nanoemulsions on injured vascular endothelial cells, we constructed an HG-induced endothelial cell injury model. The blank nanoemulsions (equivalent to 40 μg/L BSA) or the free EOFAZ (0.125–16 μg/mL) showed no toxicity to HUVECs, indicating good safety and biocompatibility (Fig. S6). When the D-Glucose concentration was 35 mM, the activity of HUVECs decreased to 71 % (Fig. 5A). Based on the previous studies [57], D-Glucose of 35 mM was used as the model concentration. Subsequently, it was shown that EOFAZ concentration of 1 μg/L could effectively reverse the damage of 35 mM D-Glucose to HUVECs, and the cell activity recovered from approximately 70 % to 81 % (Fig. 5B). Therefore, we selected 1 μg/L EOFAZ as the dose of cell experiment to investigate the effect and mechanism of EOFAZ *in vitro*. As shown in Fig. 5C, it was found that the EOFAZ@BD$_5$/S could enhance the protective effect of EOFAZ to maintain 85.07 ± 0.92 % cell viability in HUVECs. In addition, we also stained HUVECs with trypan blue to observe the effects of HG on HUVEC cell activity and cell membrane integrity (Fig. 5D, G). Cells that are normally inactive or have an imperfect cell membrane with enhanced permeability, can be stained by trypan blue. Normally, trypan blue-stained cells can be considered dead cells. The number of dead cells in the model group increased by 30.28 % compared with that in the control group. Among free EOFAZ and EOFAZ nanoemulsion groups, the EOFAZ@BD$_5$/S group had the least number of dead cells stained, which proved that EOFAZ@BD$_5$/S could significantly increase the effect of EOFAZ on maintaining HUVEC vitality. Endothelial cell migration is a hallmark of angiogenesis and vascular repair [58]. To investigate the effect of free EOFAZ and EOFAZ nanoemulsions on endothelial cell migration *in vitro*, we performed a wound healing assay. The results illustrated that HG inhibited wound healing *in vitro*, while free EOFAZ and EOFAZ nanoemulsions rescued healing (Fig. 5E, H). Compared with the model group, the migration distance of the free EOFAZ, EOFAZ@B, EOFAZ@BD$_5$ and EOFAZ@BD$_5$/S groups increased by 4.11 %, 12.80 %, 18.34 % and 26.60 %, respectively. EOFAZ@BD$_5$/S showed the strongest promotion effect on wound healing *in vitro*. Vascular endothelial cell tube formation is one of the indicators used to evaluate the functional integrity of vascular endothelial cells [59]. As shown in Fig. 5F and I, it was demonstrated that the free EOFAZ and EOFAZ nanoemulsions enhanced the tube formation ability of HUVECs under HG conditions, while EOFAZ@BD$_5$/S exhibited the strongest promoting effect of tube formation. The above dates indicate that the EOFAZ@BD$_5$/S not only reduces the structural damage of HG to vascular endothelial cells, but also restores the function of HG-damaged

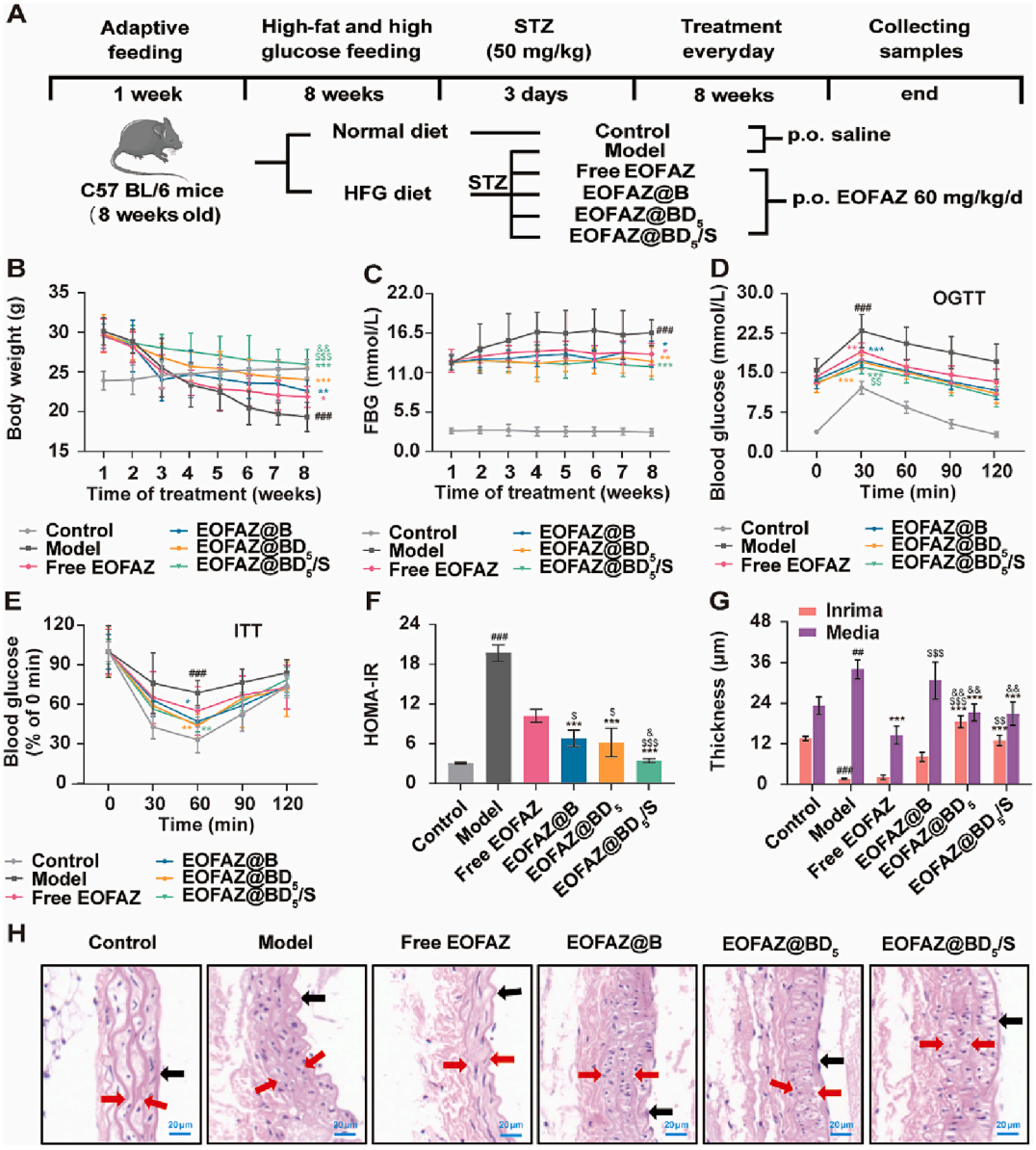

Fig. 7. Evaluation of treatment effects by EOFAZ nanoemulsions on T_2DM mice of vascular injury. (A) Schematic diagram of T_2DM mice of vascular injury model replication and treatments schedule. Variation on (B) body weight and (C) FBG of mice during the treatments ($n = 7$). (D) OGTT, (E) ITT and (F) HOMA-IR were measured after treatment. HOMA-IR = FBG value × fasting serum insulin value/22.5. (G) Statistical analysis of data on the intimal and medial layer thickness of the thoracic artery in each group. (H) Morphology and histologic analysis of thoracic aorta tissues of mice by H&E stain (×40, scale bar reads 20 μm, black arrows indicate the intima and medial layer is the area between the two red arrows). Data were shown as mean ± SD ($n = 3$). $^{\#}p < 0.05$, $^{\#\#}p < 0.01$ and $^{\#\#\#}p < 0.001$ relative to control, $^{*}p < 0.05$, $^{**}p < 0.01$ and $^{***}p < 0.001$ relative to model, $^{\$}p < 0.05$, $^{\$\$}p < 0.01$ and $^{\$\$\$}p < 0.001$ relative to free EOFAZ, $^{\&}p < 0.05$, $^{\&\&}p < 0.01$ and $^{\&\&\&}p < 0.001$ relative to EOFAZ@B.

vascular endothelial cells, so as to better play the protective effect of EOFAZ on vascular endothelial cells.

Further study showed that EOFAZ nanoemulsions had better antioxidant and anti-inflammatory activity than free EOFAZ (Fig. 6). Firstly, EOFAZ nanoemulsions could significantly up-regulate the expression of antioxidant proteins by activating the expression of Nrf2 and alleviate the oxidative stress of HG-damaged vascular endothelial cells (Fig. 6A, B). The antioxidant capacity of EOFAZ nanoemulsions was also evidenced by the detection of oxidative stress-related indexes in HG-damaged HUVECs. It was found that EOFAZ nanoemulsions up-regulated the activity of SOD and the expression level of GSH (Fig. 6D, E), and thus alleviated intracellular ROS accumulation (Fig. S7). The down-regulation of intracellular ROS can also reduce the oxidation of lipids to form MDA, so that the MDA content in HUVECs treated by EOFAZ nanoemulsions is significantly decreased compared with that in the free EOFAZ or model group (Fig. 6F). Besides, EOFAZ nanoemulsions can also inhibit inflammatory response caused by vascular endothelial cell injury *via* inhibiting the NF-κB expression (Fig. 6A, C). After treatment with EOFAZ nanoemulsions, the secretion of pro-inflammatory cytokines such as IL-1β, IL-6 and TNF-α was significantly reduced in HG-damaged HUVECs (Fig. 6G–I). In general, EOFAZ nanoemulsions, especially the EOFAZ@BD_5/S group, enhanced the antioxidant and anti-inflammatory effects of EOFAZ on HG injured HUVECs.

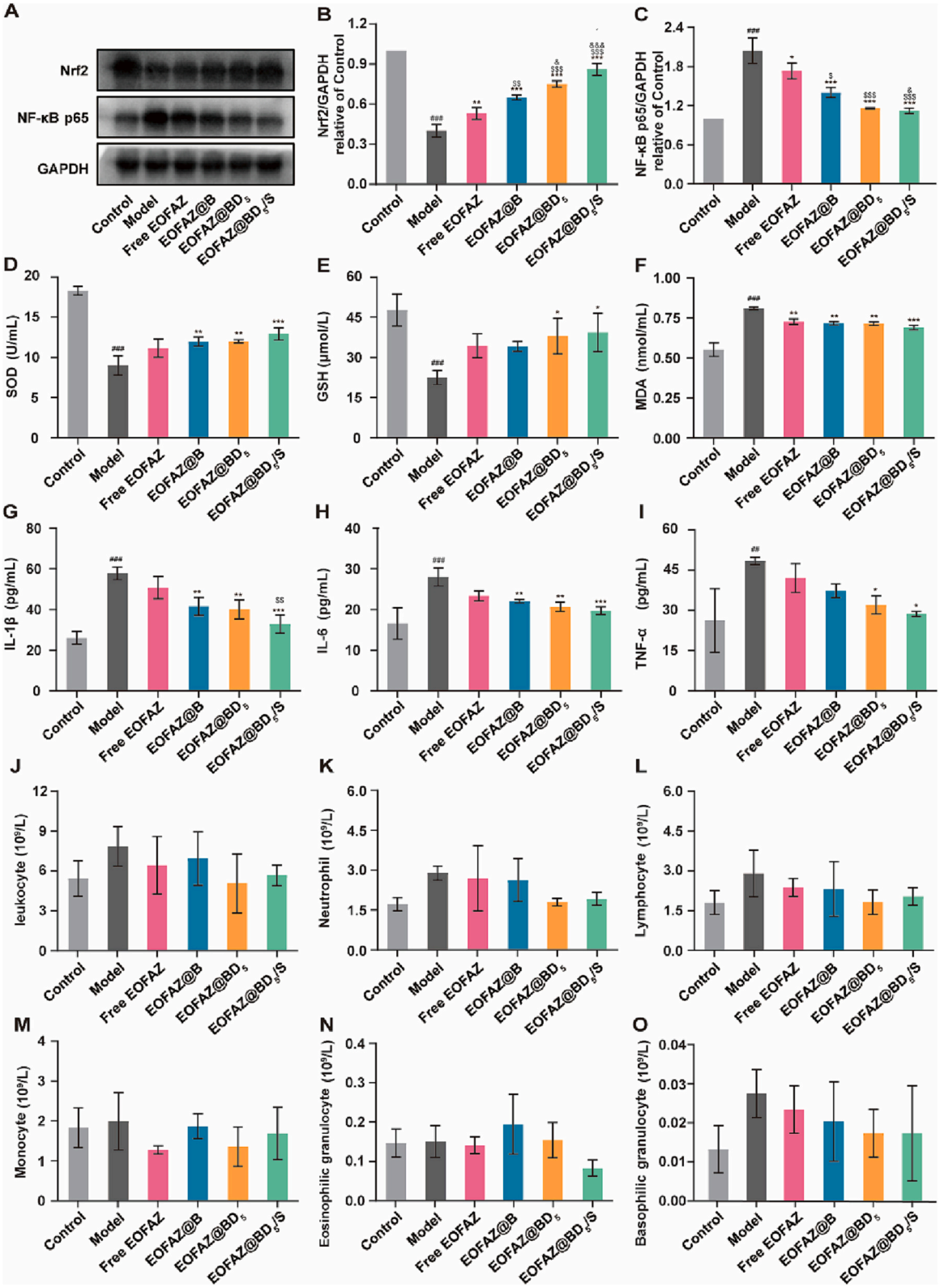

Fig. 8. Protective role of EOFAZ in vascular injury by inhibiting oxidative stress and inflammation. (A) The expression of Nrf2 and NF-κB p65 in thoracic aorta were detected by western blot and (B and C) quantitative analysis by densitometry. Expressed relative to GAPDH. The expression of (D) SOD, (E) GSH, (F) MDA, (G) IL-1β, (H) IL-6 and (I) TNF-α in serum were measured by ELISA. Levels of inflammatory cells in the blood of T_2DM mice treated with EOFAZ nanoemulsions, (J) leukocyte, (K) neutrophil, (L) lymphocyte, (M) monocyte, (N) eosinophilic granulocyte and (O) basophilic granulocyte number of mice. Data were shown as mean ± SD ($n = 3$). $^{\#}p < 0.05$, $^{\#\#}p < 0.01$ and $^{\#\#\#}p < 0.001$ relative to control, $^{*}p < 0.05$, $^{**}p < 0.01$ and $^{***}p < 0.001$ relative to model, $^{\$}p < 0.05$, $^{\$\$}p < 0.01$ and $^{\$\$\$}p < 0.001$ relative to free EOFAZ, $^{\&}p < 0.05$, $^{\&\&}p < 0.01$ and $^{\&\&\&}p < 0.001$ relative to EOFAZ@B, $^{\delta}p < 0.05$, $^{\delta\delta}p < 0.01$ and $^{\delta\delta\delta}p < 0.001$ relative to EOFAZ@BD$_5$.

3.7. Therapeutic effects of EOFAZ-loaded nanoemulsions on diabetes-induced endothelial injury

Previous studies have shown that vascular endothelial injury is the initiating factor and key link in the development and deterioration of cardiovascular complications in DM, and endothelial cell dysfunction generally occurs at the early stage of DM [60,61]. To investigate study the protective effects of EOFAZ-loaded nanoemulsions on vascular injury, the T_2DM mouse model was established by HFG combined with STZ, and normal diet-fed mice were used as control group (Fig. 7A) [62].

We first investigated the contents of EOFAZ in the blood of T_2DM mice 1 h after administration of free EOFAZ and EOFAZ nanoemulsions (Method S8). The EOFAZ component analysis before and after entering the blood is shown in Table S2 and Table S6. Before entering the blood, the percentage contents of the four main active components α-pinene, camphene, β-pinene and 1,8-cineole of free EOFAZ were 3.83 ± 0.21 %, 1.82 ± 0.14 %, 6.93 ± 0.15 % and 4.54 ± 0.27 %, respectively. After oral administration of free EOFAZ, the percentage contents of the four main active components in the plasma of mice were decreased to 1.98 ± 1.02 %, 1.01 ± 0.50 %, 2.16 ± 0.82 % and 1.49 ± 0.60 %, respectively. After oral administration of EOFAZ nanoemulsions, the percentage contents of the main active ingredients in the plasma of mice also changed to different degrees. Among them, the percentage contents of α-pinene, camphene, β-pinene and 1,8-cineole in EOFAZ@BD_5/S group decreased from 3.95 ± 0.18 %, 1.74 ± 0.13 %, 6.87 ± 0.16 % and 4.57 ± 0.11 % to 2.39 ± 0.82 %, 1.18 ± 0.0.51 %, 2.46 ± 0.80 % and 1.69 ± 0.57 %, respectively. The concentrations of the four main active components in the plasma at 1 h after oral administration (Table S7). Compared with the free EOFAZ group, the concentrations of α-pinene, camphene, β-pinene and 1,8-cineole in the plasma of mice were increased by EOFAZ nanoemulsions to varying degrees. The concentration of α-pinene, camphene, β-pinene, 1,8-cineole in EOFAZ@BD_5/S group were increased by 1.41, 1.47, 1.48 and 1.37 times, respectively compared with the free EOFAZ group. These results indicate that nanoemulsion can improve the oral absorption of the active ingredients of EOFAZ to a certain extent, which further validates the potential of nanoemulsion as an oral delivery carrier for hydrophobic essential oil drugs.

Subsequently, T_2DM mice were treated orally at a dose of 60 mg/kg EOFAZ for 8 weeks. To evaluate the therapeutic effect of different EOFAZ nanoemulsions on vascular endothelial injury caused by diabetes. It was found that the rapid body weight loss of T_2DM mice was alleviated by the oral administration of EOFAZ nanoemulsions (Fig. 7B). With the FBG was detected during the treatments. The model group exhibited a high level of FBG at 12.5–16.7 mmol/L. After the intervention by EOFAZ-loaded nanoemulsions, the FBG of EOFAZ@BD_5 and EOFAZ@BD_5/S groups increased slowly (Fig. 7C). Previous studies have shown that EOFAZ may ameliorate oxidation imbalance to reverse or restore islet β cell function [63], which was supposed to contribute to blood glucose control. After 8 weeks of treatment, the OGTT was carried out in different groups (Fig. 7D). The oral glucose tolerance test (OGTT) is the gold standard for the diagnosis of diabetes [64,65]. The highest glucose value of the model group was much higher than control group, indicating the poor ability of mice to regulate glucose, which confirmed the successful establishment of the T_2DM mouse model. After oral administration of EOFAZ nanoemulsions, the blood glucose level was maintained in 12.0–14.3 mmoI/L, indicating partial recovery of glucose regulation ability. The studies of ITT and HOMA-IR further evaluate the sensitivity of mice to insulin. It was indicated that EOFAZ nanoemulsions may restore the insulin sensitivity of T_2DM mice that contributed to blood glucose regulation (Fig. 7E, F).

Histological analysis of the thoracic aorta in mice suggested that hyperglycemia could induce vascular endothelial injury, a disorder of elastic fibers in the tunica media, degeneration of intimal eminence, and obvious surface lesions in T_2DM mice. After 8 weeks of treatment, the injury of the aortic vessels was relieved to different degrees (Fig. 7H). EOFAZ@BD_5/S significantly alleviated the injured vascular endothelium indicated by reduced intima surface injury and the thickness of the tunica media (Fig. 7G). Inflammatory cells are widely distributed in the intima-media of the blood vessel walls, and the tunica media of the blood vessel wall of T_2DM mice are thickened to varying degrees, which may be related to the inflammatory response [66]. Furthermore, the expression level of Nrf2 and NF-κB p65 were detected and quantified (Fig. 8A–C). The levels of oxidative stress-related indexes (SOD, GSH and MDA) and pro-inflammatory factors (IL-1β, IL-6 and TNF-α) were monitored after treatments (Fig. 8D–I). The changes of different cells in the abdominal aorta blood of model mice after administration in different groups were measured (Fig. 8J–O). The results showed that inflammatory cells, including leukocyte, neutrophil, lymphocyte, monocyte, eosinophilic granulocyte and basophilic granulocyte, were increased to varying degrees in the model group. EOFAZ nanoemulsion lower these cells, although there was no significant statistical difference, probably due to the small sample size. These results suggest that free EOFAZ and its nanoemulsion may reduce the recruitment of leukocytes in the vascular region by down-regulating the secretion of inflammatory cytokines. It was clarified that EOFAZ and its nanoemulsions could relieve the oxidative stress of HG-induced vascular endothelial cells by up-regulating the level of Nrf2 and prevent inflammatory-induced vascular endothelial injury by down-regulating the level of NF-κB. It was demonstrated that EOFAZ@BD_5/S achieved the most impressive protective effect against HG-induced vascular endothelial injury by improving the stability, oral bioavailability and targeting capability of free EOFAZ. In addition, we assessed the safety of EOFAZ and EOFAZ nanoemulsions treatments *via* tissue morphology observation (Fig. S8D) and blood routine detection (Fig. S8A—C). The results suggested that EOFAZ treatments exhibited no toxicity in the mice.

4. Conclusions

To conclude, vascular endothelial injury is a key point and initiating factor in the development and deterioration of diabetic cardiovascular complications. The development of an effective oral drug delivery system for treating vascular endothelial injury induced by hyperglycemia is urgently needed. We designed and constructed a nanoemulsion prepared by BD_5 and SD. The nanoemulsion has a longer gastrointestinal retention time, is easier to penetrate the gastrointestinal barrier, can be absorbed and has a longer systemic circulation time. In addition, the nanoemulsion successfully loaded EOFAZ, a vascular endothelial protection drug. EOFAZ@BD_5/S improved the stability of EOFAZ *in vitro* and *in vivo*, and enhanced the protective effect of EOFAZ on vascular endothelial injury induced by hyperglycemia by improving oxidative stress and inhibiting inflammation. This study provides a new strategy for the treatment of hyperglycemic-induced vascular endothelial injury, and also provides a nanodelivery platform for the application of essential oils in oral drug delivery protocols.

CRediT authorship contribution statement

Jinzhuan Xu: investigation, visualization, formal analysis, data curation, writing and editing. Zhaohui Jiang: investigation and validation, funding acquisition. Jianqing Peng: investigation, writing, review and editing. Runbin Sun: investigation and validation. Lili Zhang: investigation. Yan Chen: investigation. Di Pan: investigation. Jing Huang: review and editing. Zipeng Gong: methodology, conceptualization and supervision. Yi Chen: original draft writing, supervision, project administration, funding acquisition. Xiangchun Shen: conceptualization, methodology, supervision, funding acquisition.

Declaration of competing interest

The authors declared no competing interests.

Acknowledgments

This work was supported by the National Natural Science Foundation of China [82104537, 82260827]; the Excellent Young Talents Plan of Guizhou Medical University [2020-102, 2021-103, 2022-104]; Science and Technology Planning Project of Guizhou Province [qiankehejichu (2020)1Z069, qiankehejichu-ZK(2021)566]; Guiyang Science and Technology Planning Project [zhukehetong(2021)43-23]; Natural Science Research Foundation of Guizhou Provincial Department of Education (qianjiaoji[2023]066); the Excellent Young Talents Plan of Guizhou Province (QKHPTRC-YQK[2023]029, QKHPTRC(2021)-5632).

Appendix A. Supplementary data

Supplementary data to this article can be found online at https://doi.org/10.1016/j.ijbiomac.2023.125918.

References

[1] Y. Liu, S. Zeng, W. Ji, H. Yao, L. Lin, H. Cui, H.A. Santos, G. Pan, Emerging theranostic nanomaterials in diabetes and its complications, Adv. Sci. (Weinh). 9 (2022), e2102466.
[2] H. Sun, P. Saeedi, S. Karuranga, M. Pinkepank, K. Ogurtsova, B. Duncan, C. Stein, A. Basit, J. Chan, J. Mbanya, M. Pavkov, A. Ramachandaran, S. Wild, S. James, W. Herman, P. Zhang, C. Bommer, S. Kuo, E. Boyko, D. Magliano, IDF diabetes atlas: global, regional and country-level diabetes prevalence estimates for 2021 and projections for 2045, Diabetes Res. Clin. Pract. 183 (2022), 109119.
[3] T. Bhamidipati, M. Kumar, S.S. Verma, S.K. Mohanty, S. Kacar, D. Reese, M. M. Martinez, M.M. Kamocka, K.W. Dunn, C.K. Sen, K. Singh, Epigenetic basis of diabetic vasculopathy, Front. Endocrinol. 13 (2022), 989844.
[4] T. Geng, K. Zhu, Q. Lu, Z. Wan, X. Chen, L. Liu, A. Pan, G. Liu, Healthy lifestyle behaviors, mediating biomarkers, and risk of microvascular complications among individuals with type 2 diabetes: a cohort study, PLoS Med. 20 (2023), e1004135.
[5] P. Dhawan, S. Vasishta, A. Balakrishnan, M.B. Joshi, Mechanistic insights into glucose induced vascular epigenetic reprogramming in type 2 diabetes, Life Sci. 298 (2022), 120490.
[6] M. Li, B. Han, H. Zhao, C. Xu, D. Xu, S. Elwira, X. Lin, G. Kai, Biological active ingredients of Astragali Radix and its mechanisms in treating cardiovascular and cerebrovascular diseases, Phytomedicine 98 (2022), 153918.
[7] J. Li, X. Li, C. Wang, M. Zhang, M. Ye, Q. Wang, The potential of Valeriana as a traditional Chinese medicine: traditional clinical applications, bioactivities, and phytochemistry, Front. Pharmacol. 13 (2022), 973138.
[8] Q. Zhao, L. Zhu, S. Wang, Y. Gao, F. Jin, Molecular mechanism of the anti-inflammatory effects of plant essential oils: a systematic review, J. Ethnopharmacol. 301 (2023), 115829.
[9] T.M. Osaili, D.K. Dhanasekaran, F. Zeb, M.E. Faris, N. Farah, R. Hadia, C.I. Leila, H. Hayder, H. Mona, O.R. Shaker, A status review on health-promoting properties and global regulation of essential oils, Molecules 28 (2023) 1809.
[10] P.S.A. Cláudia, F. Laura, P. Diana, S. Fernando, S.M. João, Z. Mahdi, Z. Hajra, Cyclodextrins as an encapsulation molecular strategy for volatile organic compounds- pharmaceutical applications, Colloids Surf. B Biointerfaces 218 (2022), 112758.
[11] Z. Mónica, V. Carla, S. Lígia, G. Henrique, Plant nanovesicles for essential oil delivery, Pharmaceutics 14 (2022) 2581.
[12] J. Chen, S. Li, Q. Zheng, X. Feng, W. Tan, K. Feng, Y. Liu, W. Hu, Preparation of solid lipid nanoparticles of cinnamaldehyde and determination of sustained release capacity, Nanomaterials (Basel) 12 (2022) 4460.
[13] S.F. Sadeghian, M. Majdinasab, M. Nejadmansouri, S.M.H. Hosseini, Effects of natural antioxidants and high-energy fabrication methods on physical properties and oxidative stability of flaxseed oil-in-water nanoemulsions, Ultrason. Sonochem. 92 (2023), 106277.
[14] F. Salehi, H. Behboudi, E. Salehi, S.K. Ardestani, F. Piroozmand, G. Kavoosi, Zataria multiflora apple pectin-based essential oil (ZEO) nanoemulsion: an approach to enhance ZEO DNA damage induction in breast cancer cells as and studies reveal, Front. Pharmacol. 13 (2022), 946161.
[15] S.A. Razack, Y. Lee, H. Shin, S. Duraiarasan, B.S. Chun, H.W. Kang, Cellulose nanofibrils reinforced chitosan-gelatin based hydrogel loaded with nanoemulsion of oregano essential oil for diabetic wound healing assisted by low level laser therapy, Int. J. Biol. Macromol. 226 (2023) 220–239.
[16] M.V. Dinu, A.C. Gradinaru, M.M. Lazar, I.A. Dinu, I.E. Raschip, N. Ciocarlan, A. C. Aprotosoaie, Physically cross-linked chitosan/dextrin cryogels entrapping Thymus vulgaris essential oil with enhanced mechanical, antioxidant and antifungal properties, Int. J. Biol. Macromol. 184 (2021) 898–908.
[17] K.M. Hosny, A.M. Sindi, H.M. Alkhalidi, M. Kurakula, N.K. Alruwaili, N. A. Alhakamy, W.A. Abualsunun, R.B. Bakhaidar, R.H. Bahmdan, W.Y. Rizg, S. A. Ali, W.H. Abdulaal, M.S. Nassar, M.S. Alsuabeyl, A.F. Alghaith, S. Alshehri, Oral gel loaded with penciclovir-lavender oil nanoemulsion to enhance bioavailability and alleviate pain associated with herpes labialis, Drug Deliv. 28 (2021) 1043–1054.
[18] R. Ebrahimi, M. Fathi, H.B. Ghoddusi, Nanoencapsulation of oregano essential oil using cellulose nanocrystals extracted from hazelnut shell to enhance shelf life of fruits: case study: pears, Int. J. Biol. Macromol. 242 (2023), 124704.
[19] F.G. Liu, M.C.D. Julian, M. Cuicui, X.B. Liu, Novel colloidal food ingredients: protein complexes and conjugates, Annu. Rev. Food Sci. Technol. 14 (2023) 35–61.
[20] Y. Zhou, S.P. Petrova, K.J. Edgar, Chemical synthesis of polysaccharide-protein and polysaccharide-peptide conjugates: a review, Carbohydr. Polym. 274 (2021), 118662.
[21] A. Aguilera-Garrido, T. Del Castillo-Santaella, Y. Yang, F. Galisteo-González, M. J. Gálvez-Ruiz, J.A. Molina-Bolívar, J.A. Holgado-Terriza, M.Á. Cabrerizo-Vílche, J. Maldonado-Valderrama, Applications of serum albumins in delivery systems: differences in interfacial behaviour and interacting abilities with polysaccharides, Adv. Colloid Interf. Sci. 290 (2021), 102365.
[22] D. Zhao, Y. Ge, X. Xiang, H. Dong, W. Qin, Q. Zhang, Structure and stability characterization of pea protein isolate-xylan conjugate-stabilized nanoemulsions prepared using ultrasound homogenization, Ultrason. Sonochem. 90 (2022), 106195.
[23] N. Li, Q. Zhong, Impacts of preparation conditions on the structure and emulsifying properties of casein-alginate conjugates produced by transacylation reaction, Int. J. Biol. Macromol. 201 (2022) 242–253.
[24] S.W.K. Hansen, K. Ohtani, N. Roy, N. Wakamiya, The collectins CL-L1, CL-K1 and CL-P1, and their roles in complement and innate immunity, Immunobiology 221 (2016) 1058–1067.
[25] L. Selman, K. Skjodt, O. Nielsen, C. Floridon, U. Holmskov, S. Hansen, Expression and tissue localization of collectin placenta 1 (CL-P1, SRCL) in human tissues, Mol. Immunol. 45 (2008) 3278–3288.
[26] S. Jang, K. Ohtani, A. Fukuoh, T. Yoshizaki, M. Fukuda, W. Motomura, K. Mori, J. Fukuzawa, N. Kitamoto, I. Yoshida, Y. Suzuki, N. Wakamiya, Scavenger receptor collectin placenta 1 (CL-P1) predominantly mediates zymosan phagocytosis by human vascular endothelial cells, J. Biol. Chem. 284 (2009) 3956–3965.
[27] Y. Gao, Y. He, H. Zhang, Y. Zhang, T. Gao, J. Wang, S. Wang, Zwitterion-functionalized mesoporous silica nanoparticles for enhancing oral delivery of protein drugs by overcoming multiple gastrointestinal barriers, J. Colloid Interface Sci. 582 (2021) 364–375.
[28] Z. Xi, E. Ahmad, W. Zhang, J. Li, A. Wang, N. Faridoon, C. Wang, W. Zhu, L. Huang, M. Xu, Y. Gan Yu, Dual-modified nanoparticles overcome sequential absorption barriers for oral insulin delivery, J. Control. Release 342 (2022) 1–13.
[29] Y. Liu, J. Liu, J. Liang, M. Zhang, Z. Li, Z. Wang, B. Dang, N. Feng, Mucosal transfer of wheat germ agglutinin modified lipid-polymer hybrid nanoparticles for oral delivery of oridonin, Nanomedicine 13 (2017) 2219–2229.
[30] W. Fan, D. Xia, Q. Zhu, X. Li, S. He, C. Zhu, S. Guo, L. Hovgaard, M. Yang, Y. Gan, Functional nanoparticles exploit the bile acid pathway to overcome multiple barriers of the intestinal epithelium for oral insulin delivery, Biomaterials 151 (2018) 13–23.
[31] L. Wang, Q. Liu, X. Hu, C. Zhou, Y. Ma, X. Wang, Y. Tang, K. Chen, X. Wang, Y. Liu, Enhanced oral absorption and liver distribution of polymeric nanoparticles through traveling the enterohepatic circulation pathways of bile acid, ACS Appl. Mater. Interfaces 14 (2022) 41712–41725.
[32] Y. Ji, T. Shi, Y. Zhang, D. Lin, K. Linghu, Y. Xu, L. Tao, Q. Lu, X. Shen, Essential oil from Fructus *Alpinia zerumbet* (fruit of *Alpinia zerumbet* (Pers.) burtt.Et smith) protected against aortic endothelial cell injury and inflammation *in vitro* and in *vivo*, J. Ethnopharmacol. 237 (2019) 149–158.
[33] Y. Zhang, S. Zhao, M. Tu, L. He, Y. Xu, S. Gan, X. Shen, Inhibitory effect of essential oil from Fructus of *Alpinia zerumbet* on endothelial-to-mesenchymal transformation induced by TGF-β1 and downregulation of KLF4, J. Cardiovasc. Pharmacol. 80 (2022) 82–94.
[34] N. Huang, Y. Xu, H. Zhou, D. Lin, B. Zhang, Y. Zhang, D. Pan, L. Tao, X. Liu, X. Shen, Essential oil from Fructus *Alpiniae zerumbet* protects human umbilical vein endothelial cells *in vitro* from injury induced by high glucose levels by suppressing nuclear transcription factor-kappa B signaling, Med. Sci. Monit. 23 (2017) 4760–4767.
[35] T. Xiao, Y. Zeng, Y. Xu, Y. Zhang, Y. Jiang, L. Tao, X. Shen, The endothelial protective properties of essential oil from Fructus *Alpiniae zerumbet via* the Akt/NOS-NO signaling pathway *in vitr*o, Planta Med. 80 (2014) 1628–1634.
[36] Z. Jiang, X. Guo, K. Zhang, G. Sekaran, B. Cao, Q. Zhao, S. Zhang, G.M. Kirby, X. Zhang, The essential oils and eucalyptol from artemisia vulgaris L. prevent acetaminophen-induced liver injury by activating Nrf2-Keap1 and enhancing APAP clearance through non-toxic metabolic pathway, Front. Pharmacol. 10 (2019) 782.
[37] N. Lammari, O. Louaer, A.H. Meniai, A. Elaissari, Encapsulation of essential oils via nanoprecipitation process: overview, progress, challenges and prospects, Pharmaceutics 12 (2020) 431.
[38] P.M. Albuquerque, S.G. Azevedo, C.P. de Andrade, N.C. D'Ambros, M.T. Pérez, L. Manzato, Biotechnological applications of nanoencapsulated essential oils: a review, Polymers (Basel). 14 (2022) 5495.
[39] S.F. Pereira, A. Barroso, R.H.V. Mourão, C.P. Fernandes, A low energy approach for the preparation of nano-emulsions with a high citral-content essential oil, Molecules 26 (2021) 3666.
[40] J. Jampilek, K. Kralova, Anticancer applications of essential oils formulated into lipid-based delivery nanosystems, Pharmaceutics 14 (2022) 2681.
[41] M. Zhang, R.A. Hutchinson, Innovative process for facile dextran-bovine serum albumin conjugate synthesis: mechanism, kinetics and characterization, Carbohydr. Polym. 295 (2022), 119850.
[42] J. Xiang, F. Liu, B. Wang, L. Chen, W. Liu, S. Tan, A literature review on maillard reaction based on milk proteins and carbohydrates in food and pharmaceutical products: advantages, disadvantages and avoidance strategies, Foods 10 (2021) 1998.

[43] S. Haddadzadegan, F. Dorkoosh, A. Bernkop-Schnürch, Oral delivery of therapeutic peptides and proteins: technology landscape of lipid-based nanocarriers, Adv. Drug Deliv. Rev. 182 (2022), 114097.
[44] S.S. Srinivasan, A. Alshareef, A.V. Hwang, Z. Kang, J. Kuosmanen, K. Ishida, J. Jenkins, S. Liu, W.A.M. Madani, J. Lennerz, A. Hayward, J. Morimoto, N. Fitzgerald, R. Langer, G. Traverso, RoboCap: robotic mucus-clearing capsule for enhanced drug delivery in the gastrointestinal tract, Sci. Robot. 7 (2022) eabp9066.
[45] W. Li, Y. Zhou, N. Pang, Q. Hu, Q. Li, Y. Sun, Y. Ding, Y. Gu, Y. Xiao, M. Gao, S. Ma, J. Pan, E.F. Fang, Z. Zhang, L. Yang, NAD supplement alleviates intestinal barrier injury induced by ethanol *via* protecting epithelial mitochondrial function, Nutrients. 15 (2022) 174.
[46] L. Dong, J. Xie, Y. Wang, H. Jiang, K. Chen, D. Li, J. Wang, Y. Liu, J. He, J. Zhou, L. Zhang, X. Lu, X. Zou, X. Wang, Q. Wang, Z. Chen, D. Zuo, Mannose ameliorates experimental colitis by protecting intestinal barrier integrity, Nat. Commun. 13 (2022) 4804.
[47] Z. Niu, I. Thielen, A. Barnett, S.M. Loveday, H. Singh, ε-Polylysine and β-cyclodextrin assembling as delivery systems for gastric protection of proteins and possibility to enhance intestinal permeation, J. Colloid Interface Sci. 546 (2019) 312–323.
[48] B. Hasannejad-Asl, F. Pooresmaeil, S. Takamoli, M. Dabiri, A. Bolhassani, Cell penetrating peptide: a potent delivery system in vaccine development, Front. Pharmacol. 13 (2022) 1072685.
[49] D. Manzanares, M.D. Pérez-Carrión, J.L. Jiménez Blanco, C. Ortiz Mellet, J. M. García Fernández, V. Ceña, Cyclodextrin-based nanostructure efficiently delivers siRNA to glioblastoma cells preferentially *via* macropinocytosis, Int. J. Mol. Sci. 21 (2020) 9306.
[50] C. Wang, Y. Zhang, Z. Wang, Y. Li, Q. Guan, D. Xing, W. Zhang, Design, synthesis, and biological evaluation of biotinylated colchicine derivatives as potential antitumor agents, J. Enzyme Inhib. Med. Chem. 37 (2022) 411–420.
[51] K. Ohtani, Y. Suzuki, S. Eda, T. Kawai, T. Kase, H. Keshi, Y. Sakai, A. Fukuoh, T. Sakamoto, H. Itabe, T. Suzutani, M. Ogasawara, I. Yoshida, N. Wakamiya, The membrane-type collectin CL-P1 is a scavenger receptor on vascular endothelial cells, J. Biol. Chem. 276 (2001) 44222–44228.
[52] Y. Chen, D. Li, Y. Xu, Y. Zhang, L. Tao, S. Li, Y. Jiang, X. Shen, Essential oils from Fructus *A. zerumbet* protect human aortic endothelial cells from apoptosis induced by Ox-LDL *in vitro*, Evid. Based Complement Alternat Med. 2014 (2014) 956824.
[53] Y. Zhang, C. Li, Y. Huang, S. Zhao, Y. Xu, Y. Chen, F. Jiang, L. Tao, X. Shen, EOFAZ inhibits endothelial-to-mesenchymal transition through downregulation of KLF4, Int. J. Mol. Med. 46 (2020) 300–310.
[54] T.A. de Souza, M.B.P. Lopes, A.S. Ramos, J.L.P. Ferreira, J.R.A. Silva, M.M. C. Queiroz, K.G.L. Araújo, A.C.F. Amaral, *Alpinia* essential oils and their major components against, a vector of chagas disease, Sci. World J. 2018 (2018) 2393858.
[55] X. Shen, H. Hu, H. Xiao, GC-MS analysisi of chemical constituents of the essential oil from different parts of *Alpinia zerumbet* (Pers.) Burtt smith, Chin. J. Pharm. Anal. 30 (2010) 1399–1403.
[56] L. Tao, H.S. Hu, X.C. Shen, Endothelium-dependent vasodilatation effects of the essential oil from Fructus *Alpiniae zerumbet* (EOFAZ) on rat thoracic aortic rings *in vitro*, Phytomedicine 20 (2013) 387–393.
[57] N. Huang, Y. Xu, H. Zhou, D. Lin, B.Y. Zhang, D. Zhang, L. Pan, X. Tao, X. Liu, X. Shen, Essential oil from Fructus *Alpiniae zerumbet* protects human umbilical vein endothelial cells *in vitro* from injury induced by high glucose levels by suppressing nuclear transcription factor-kappa B signaling, Med. Sci. Monit. 23 (2017) 4760–4767.
[58] J. Zhang, S.H. Chen, H. Xiang, J. Xiao, S.L. Zhao, Z.H. Shu, Y.F. Chai, J. Ouyang, H. Q. Liu, X.W. Wang, Q.S. Quan, J.N. Fan, P. Gao, A.F. Chen, H.W. Lu, S1PR2/Wnt3a/RhoA/ROCK1/β-catenin signaling pathway promotes diabetic nephropathy by inducting endothelial mesenchymal transition and impairing endothelial barrier function, Life Sci. 328 (2023), 121853.
[59] F.Y. Li, X. Gou, D. Xu, K. Hou, W.R. Fang, Y.M. Li, Improvement of tube formation model of cell: application for acute hypoxia in *in vitro* study of angiogenesis, Microvasc. Res. 140 (2022), 104297.
[60] J. Wils, J. Favre, J. Bellien, Modulating putative endothelial progenitor cells for the treatment of endothelial dysfunction and cardiovascular complications in diabetes, Pharmacol. Ther. 170 (2017) 98–115.
[61] W.A. Hsueh, S. Jackson, R.E. Law, Control of vascular cell proliferation and migration by PPAR-gamma: a new approach to the macrovascular complications of diabetes, Diabetes Care 24 (2001) 392–397.
[62] Q. Zhang, R. Li, L. Wang, T. Zhang, D. Qian, D. Tang, C. He, C. Wu, L. Ai, Zanthoxylum bungeanumHydroxy-α-sanshool isolated from maxim. has antidiabetic effects on high-fat-fed and streptozotocin-treated mice increasing glycogen synthesis by regulation of PI3K/Akt/GSK-3β/GS signaling, Front. Pharmacol. 13 (2022) 1089558.
[63] H. Yang, T. Chen, Y. Chen, X. Song, X. Ma, B. Zhang, X. Shen, Y. Li, The protective effect of essential oil from *Alpiniae zerumbet* Fructus on T_2DM induced pancreatic injury in mice based on p62/Keap1/Nrf2 signaling pathway, Chin. Pharmacol. Bull. 38 (2022) 613–618.
[64] P.J. Phillips, Oral glucose tolerance testing, Aust. Fam. Physician 41 (2012) 391–393.
[65] C.R. Bruce, S. Hamley, A. Teddy, K.F. Howlett, C.S. Shaw, G.M. Kowalski, Translating glucose tolerance data from mice to humans: insights from stable isotope labelled glucose tolerance tests, Mol. Metab. 53 (2021), 101281.
[66] D.J. Chen, L.J. Zhong, Y. Li, R. He, C. Ding, X. Chen, W.H. Lian, Changes in serum inflammatory factor interleukin-6 levels and pathology of carotid vessel walls of rats with chronic periodontitis and diabetes mellitus after the periodontal intervention, Saudi. J. Biol. Sci. 27 (2020) 1679–1684.